1991

Characterizations of F-superconductors and selected F-compounds, amorphous carbon and (VO)2P2O7 by 19F, 13C, 1H, 31P NMR and a new probe for multiple pulse, MAS and DAS NMR

Hongjun Pan
Iowa State University

INFORMATION TO USERS

This manuscript has been reproduced from the microfilm master. UMI films the text directly from the original or copy submitted. Thus, some thesis and dissertation copies are in typewriter face, while others may be from any type of computer printer.

The quality of this reproduction is dependent upon the quality of the copy submitted. Broken or indistinct print, colored or poor quality illustrations and photographs, print bleedthrough, substandard margins, and improper alignment can adversely affect reproduction.

In the unlikely event that the author did not send UMI a complete manuscript and there are missing pages, these will be noted. Also, if unauthorized copyright material had to be removed, a note will indicate the deletion.

Oversize materials (e.g., maps, drawings, charts) are reproduced by sectioning the original, beginning at the upper left-hand corner and continuing from left to right in equal sections with small overlaps. Each original is also photographed in one exposure and is included in reduced form at the back of the book.

Photographs included in the original manuscript have been reproduced xerographically in this copy. Higher quality 6" x 9" black and white photographic prints are available for any photographs or illustrations appearing in this copy for an additional charge. Contact UMI directly to order.

UMI

University Microfilms International
A Bell & Howell Information Company
300 North Zeeb Road, Ann Arbor, MI 48106-1346 USA
313/761-4700 800/521-0600

Order Number 9126233

Characterizations of F-superconductors and selected F-compounds, amorphous carbon and $(VO)_2P_2O_7$ by ^{19}F, ^{13}C, ^{1}H, ^{31}P NMR and a new probe for multiple pulse, MAS and DAS NMR

Pan, Hongjun, Ph.D.

Iowa State University, 1991

U·M·I

300 N. Zeeb Rd.
Ann Arbor, MI 48106

Characterizations of F-superconductors and selected F-compounds, amorphous carbon and $(VO)_2P_2O_7$ by ^{19}F, ^{13}C, ^{1}H, ^{31}P NMR and a new probe for multiple pulse, MAS and DAS NMR

by

Hongjun Pan

A Dissertation Submitted to the
Graduate Faculty in Partial Fulfillment of the
Requirements for the Degree of
DOCTOR OF PHILOSOPHY

Department: Chemistry
Major: Physical Chemistry

Approved:

Signature was redacted for privacy.

In Charge of Major Work

Signature was redacted for privacy.

For the Major Department

Signature was redacted for privacy.

For the Graduate College

Iowa State University
Ames, Iowa
1991

TABLE OF CONTENTS

PURPOSES AND GENERAL INTRUDOCTION

The purposes of the current work are: (a) to use solid state nuclear magnetic resonance(NMR) techniques to characterize fluorine-containing superconductors, (b) amorphous carbon and (c) $(VO)_2P_2O_7$, and (d) to design a stable system with high spinning speed which can be used for magic angle spinning, multiple pulse decoupling, combined rotation and multiple-pulse spectroscopy (CRAMPS) and dynamic angle spinning experiments.

Future potential uses of high temperature superconductors are incredible. The transition temperature of a superconductor depends on its composition and crystal structure. It was claimed that the transition temperature would be improved by replacing O with F in 1-2-3 type superconductors. Examination of F in the F-containing superconductors is important for both theoretical study and experimental synthesis.

Amorphous carbon is a type of material. It is a semiconductor which is mechanically hard, and semi-transparent to visible light. Its electrical and optical properties depend on its composition and preparation condition. The information we learn about the structure and composition of amorphous carbon will give a guide line to understand its physical properties.

High temperature NMR experiments are desirable in the modern NMR laboratory. The conventional way to do high temperature NMR is to blow hot gas into the probe, which needs extensive dewaring. The new technique of inductive heating does not require extensive

dewaring but there still exists a problem in measuring the temperature of samples. An internal temperature standard must be found which has a known temperature dependence of the chemical shift with chemical stability at high temperature.

High resolution NMR in solids requires spinning the sample at high frequency, and also changing the rotation angle rapidly. The spinning system in a conventional single bearing probe cannot withstand rapidly changing the rotation angle. A new type of spinning system must be developed for high spinning speed (10KHz) with high stability both for long period experiments and for dynamic angle spinning.

Explanation of Dissertation Format

The structure of the thesis is briefly described as follows:

Part I: ^{19}F NMR signals of F-containing 1-2-3 type superconductors and related reference samples Ag_2F, AgF, BaF_2, YOF, YF_3, CuF_2 and EuOF are measured using static single pulse, magic angle spinning, multiple pulse decoupling, CRAMPS and spin echo mapping techniques. By comparising the signals of the superconductors to those of the references, the chemical environment of F in superconductors is determined.

Part II: The structure and composition of amorphous carbon are studied by ^{13}C solid state NMR with static single pulse excitation, magic angle spinning and CP/MAS techniques. Residual protons are examined by ^{1}H NMR both for unevacuated and evacuated samples. The upper limit of hydrogenated amorphous carbon is obtained.

Part III: The temperature dependence of the isotropic chemical shift of ^{31}P in $(VO)_2P_2O_7$ is studied. A Curie-Law-type temperature dependence was observed which can be used as an internal temperature standard for high temperature NMR.

Part IV: The construction of a spinning system with high spinning speed is presented. This system has very high stability and can be used successfully for magic angle spinning, CRAMPS and dynamic angle spinning experiments.

Bibliographies in all sections follow the style of Physical Review B to which the Part II is submitted.

PART I. A REEXAMINATION OF ^{19}F NMR IN SELECTED SOLIDS, THE CONDUCTOR Ag_2F AND REFERENCE INSULATORS FOR STUDIES OF $YBa_2Cu_3O_7$-TYPE SUPERCONDUCTORS

A reexamination of ^{19}F NMR in selected solids, the conductor Ag_2F and reference insulators for studies of $YBa_2Cu_3O_7$-type superconductors

Hongjun Pan, and B. C. Gerstein
Institute for Physical Research and Technology
and
Department of Chemistry, Iowa State University
Ames, Iowa 50011
and
Hans R. Loeliger
Ciba-Geiqy Ltd., CH 4002 Swizerland
and
T. A. Vanderah
Naval Weapons Center, Chemistry Division
Research Department, China Lake CA 93555

Supported by the U. S. Department of Energy (Basic Energy Sciences program, Chmeical Science Division), under Contrat No. W-7405-Eng-82 and the office of Naval Research.

ABSTRACT

NMR signals of ^{19}F have been measured in the polycrystalline inorganic conductor Ag_2F and in the polycrystalline insulators AgF, YOF, EuOF, YF_3, CuF_2, BaF_2 and KF to compare them to the signals found in the so-called "1-2-3-type" compounds with claimed formulas $RBa_2Cu_3O_{7-x}F_x$ (R = Y and Eu). No evidence for a Knight-shifted, built-in fluorine-signal was found in the 1-2-3-type superconductors, whereas Ag_2F shows a clearly downfield shifted ^{19}F peak with reference to AgF.

INTRODUCTION

Evidence of incorporated F in the so called "1-2-3-type", $YBa_2Cu_3O_7$-derived compounds has been cited.[1-4] The aim was to confirm an increase in T_c as Ovshinsky claimed in 1987 by substitution of F for O.[5] One expects a downfield-shifted F NMR resonance (compare: ^{17}O NMR shifts[6]) for the 1-2-3-type compounds, since they display metallic conductivity at room temperature. As a guideline for judging the line positions and shapes of fluorine incorporated in the 1-2-3-type compounds, we therefore reexamined the ^{19}F NMR signals in a metallic inorganic conductor (Ag_2F), in the insulating starting materials used to synthesize the superconductor phases (YOF, EuOF and YF_3) and in BaF_2 and CuF_2 which could be formed during the synthesis. AgF and KF were used as reference samples. There appear to be only two inorganic compounds containing fluorine and showing high metallic conductivity: (1) Silver subfluoride,[7] Ag_2F, with NMR results reported by Nishihara et al.[8] and (2) $(Ag_7O_8)^+(HF_2)^-$ reported by Hindermann.[9] Pulsed NMR of ^{19}F in solids has been reported by Vaughan et al.[10, 11] and more recently by Clark et al..[12] A number of results by CW ^{19}F NMR on anhydrous and hydrated forms of AgF,[13] on YF_3 and also on BaF_2 and KF have been reviewed by Gabuda and Zemskov.[14]

EXPERIMENTS

I. Sample Preparation and Characterization

All samples, except Ag_2F and AgF, were prepared as follows:[3] YOF and EuOF were obtained by reacting equimolar amounts of YF_3 (Reacton, 99.99%), EuF_3 (Reacton, 99.9%) and Y_2O_3 (Reacton, 99.9%) or Eu_2O_3 (Lindsay Chemicals), respectively, at 650°C for 18h in an alumina combustion boat in air. The oxyfluoride products were pure according to X-ray powder diffraction. The "$RBa_2Cu_3O_{7-x}F_x$" samples were synthesized by reacting ROF (R = Y,Eu) with $2BaCO_3$ (Mallinckrodt) and 3CuO (Matthey) in alumina combustion boats in air using heating and cooling regimes similar to those used to prepare high quality $YBa_2Cu_3O_7$.[15] In each case the major component was a $YBa_2Cu_3O_7$-like phase and BaF_2 as a minor component. CuO and R_2O_3 were sometimes detectable by X-ray diffraction. Samples of "$RBa_2Cu_3O_{7-x}F_x$" containing the least amount of BaF_2 were prepared by reacting ROF (R = Y, Eu) and $BaCO_3$ in two heating cycles with intermediate grinding: 800°C for 12h, and 875-900°C for 10h followed by cooling in 8h to room temperature. A semiquantitative X-ray diffraction analysis was carried out as follows: Mixtures of BaF_2, CuO, Y_2O_3 and $YBa_2Cu_3O_7$ in relative amounts corresponding to the products which would have been obtained assuming (I) complete conversion of the reactant fluoride to BaF_2 and (II) 50% conversion of reactant fluoride to BaF_2 were mixed and heated in the same way as the "$RBa_2Cu_3O_{7-x}F_x$" samples. The relative intensities of the diffraction peaks at d = 3.58 Å,

the strongest line in the pattern of BaF_2, were compared in these mixtures with those of the $YBa_2Cu_3O_{7-x}F_x$-like phases in order to estimate x. These results were consistent with a partial incorporation on the order of 0.2 mole of F per Mol of host. Incorporation of some fluoride in the 1-2-3-type lattice was also indicated by changes in the unit cells and iodometric analyses of average copper oxidation states.[3] The "$RBa_2Cu_3O_{7-x}F_x$"samples displayed superconducting transitions in the magnetic susceptibility versus temperature curves occuring 20-25 K lower than the reported values for $YBa_2Cu_3O_{7-\delta}$. The transition ranges are also broader and show a much weaker Meissner effect.

AgF, 99.9%, with some content of $AgF.(H_2O)_x$, and $KF.2H_2O$ were both obtained from Aldrich Chemicals. Ag_2F was prepared by the method of Poyer et al.,[16] suggested by McCarley, Ames Laboratory and Department of Chemistry, Iowa State University. The X-ray powder diffraction patterns of Ag_2F agreed with published data.[17]

II. NMR Measurements

Pulsed NMR measurements were performed on a homebuilt ^{19}F NMR probe, with the double bearing version rotors of Wind's design,[18] capable of spinning up to more than 7 KHz, in a Bruker MSL-300, operated at a frequency of 282.2 MHz, and with a 90° pulse of 2 μs duration. Fluorine-free spinner materials used were either polycarbonate or Araldite (Ciba-Geigy Ltd.,Basel,Switzerland); Torlon (DuPont) was found to contain F.

Transient techniques in NMR included: (1) single pulse excitation, either static or with Magic Angle Spinning (MAS), (2)

spin echo as Spin Echo Envelope Mapping (SEEM). SEEM involves 90_x-τ-180_y and Fourier-Transformation from the center of the echo. It is applied to obtain the line shape of wide lines. By increasing the RF frequency, with re-tuning of the probe for each new frequency, in steps from values smaller than the center-frequency to larger values, a series of spectra is obtained; the envelope of these signals maps the envelope of the broad NMR line, (3) static Multi-Pulse-Dipolar-Decoupling (MPD) or (4) CRAMPS, Combined Rotation and Multi-Pulse Decoupling using the MREV-8 sequence,[19] with cycle time t_c = 48 μs.

RESULTS

Table 1 shows the present results compared to previously reported data. Because the shift values were measured against C_6F_6, i.e. $\delta(C_6F_6) = 0$, most of the earlier results had to be converted to this reference. The results of earlier papers are referred mostly to $\delta(F_2) = 0$, the so called "Absolute Fluorine Scale". The resonance of F_2 gas lies very far downfield compared to C_6F_6. So, to convert the data of the present work to the shift region around $\delta(C_6F_6)$ requires subtractions of large numbers. For the present work $\delta(C_6F_6) - \delta(F_2)$ was taken to be -585.8 ppm.[20] This fact and the relatively large uncertainties of the CW data, mainly in earlier Russian work, explain some of the smaller discrepancies reported in Table 1.

The present results for Ag_2F and AgF lie far outside of these conversion errors. The isotropic shifts differ by a factor of about 1.5 from the published data.[8, 21] The reference AgF, supposedly of a white (to lightly yellowish) color was supplied by Aldrich Chemicals as an orange-brown material.[22] Ag_2F and AgF were both sealed in the polycarbonate NMR spinner under dry nitrogen in the absence of light. In the AgF sample, not surprisingly, therefore, instead of one, there were two well defined signals, one with high intensity at -150 ppm and a less intense peak at +38 ppm. The latter signal was assigned to the brown, hydrated form of silver fluoride, probably $AgF(H_2O)_x$ (x = 2?).[22] This assumption was confirmed by the fact, that after drying 24h in vacuum at 140°C the

peak at 38 ppm had disappeared.** The high intensity peak remained, with a slight downfield shift (at most 5 ppm) and is therefore assigned to water-free AgF.

The present results on BaF_2 agree with those of Vaughan and of Burum to within experimental error,[10, 11] whereas the older Russian CW work shows large deviations from these results. The signal of YOF under MPD shows an axial shielding tensor with principal values of $\sigma_{\perp} = 110\pm5$ ppm and $\sigma_{\parallel} = 37\pm5$ ppm (table 1). The EuOF shows a very large paramagnetic shift and could only be reasonably detected by the method of Spin-Echo-Envelop-mapping (SEEM). The measured linewidth is 800±50 ppm. For YF_3 static MPD resulted in resolving the components of the asymmetric shielding tensor to be $\sigma_{11} = 140$ ppm, $\sigma_{22} = 108$ppm and $\sigma_{33} = 82$ ppm. The calculated value of $\bar{\sigma}$ compares quite well with the measured one considering the errors of both measurement and the remarks given in the discussion (see table 1). The only earlier measurement of the chemical shift powder pattern, known to the authors, is given in a

---

** During drying at 140°C the reaction $2AgF + H_2O = Ag_2O + 2HF$ takes place and therefore the sample darkens. But HF seems not to react to form $Ag^+(FHF)^-$ since after drying, the lineshape showed no sign of a wide doublet as expected from a comparison measurement with $K^+(FHF)^-$. The water remaining in the sample of AgF after drying was only a few percent of the amount originally present in the fresh commercial sample. This fact was checked by proton NMR.

paper by Gabuda et al. with a value of $\bar{\sigma}$ differing significantly from the present value.[23] ^{19}F in CuF_2 also shows a paramagnetic shift and a linewidth of 290 ppm. The signal could only be detected by SEEM.

The present determination of the isotropic shift of dried KF agrees with reference 10, but more recent values differ by some ppm, probably on account of the recalculation from the $CFCl_3$-to the C_6F_6-scale presently used.[12] Aqueous KF solutions have been remeasured for comparison. The measurements reported in references 9 and 21 used KF solutions as reference. Also shown in earlier work is the concentration dependence of δ in these solutions. Only at very high concentrations, not used in the present work, a slight δ-decrease of about 2ppm is reported.[12, 24]

DISCUSSION

The main difference between the present results and those published earlier is found in the much larger shift values reported in the present work for Ag_2F and AgF. A scale calibration error in the earlier work could explain the discrepancy.[8, 21] Therefore calculating the expected diamagnetic shift of Ag_2F as in reference 8 the present data would yield the value of -55 ppm (i.e. 195 ppm - 250 ppm, where the latter number is the theoretically calculated Knight-shift in reference 8. Note however that the static signal of this sample is of a slightly asymmetric shape with a clearly indicated shoulder in the downfield direction (see figure 2). Within the limits of error, this asymmetry is interpreted as a small axial Knight shift anisotropy (see table 1). This assignment conforms to the axial arrangement of the nearest neighbors of the fluorine atoms in Ag_2F, which has the trigonal CdI_2 structure, $P\bar{3}m1$ (D_{3d}^3).[25]

The crystal structure of AgF is cubic and of the NaCl-type ($Fm\bar{3}m$, O_h^5) and therefore shows an isotropic shift with symmetrical lineshape.

The YOF sample seems to be of the ordinary β-modification, crystallizing in the trigonal space group $R\bar{3}m$ (D_{3d}^5). This symmetry is in agreement with the present work showing an axially symmetric chemical shift tensor. No indication of paired formation of fluorines was found.[27]

In YF_3 the present determination of an asymmetric shielding tensor can be understood from the known crystal structure of this compound,[28] showing an orthorhombic lattice with space group Pnma (D_{2h}^{16}); the unit cell contains 12 fluorine atoms, 4 of them occupy site (1) and the other 8 are positioned in a nonequivalent site (2). Each fluorine in site (1), F(1), is surrounded by 6 nearest atoms in a range of distances between 2.6 and 2.8Å; these are 5 F and 1 Y. At the second site (2), nonequivalent to site (1), each F(2) is surrounded quite differently: 2 Y lie very near, at 2.3Å and the 3 nearest F are at distances between 2.6 and 2.8Å. The local symmetry of both sites is nonaxial, but the F(2) sites would appear to be more highly anisotropic. On the other hand the unit cell contains twice as many F(2) atoms. Therefore it seems very probable that it is correct to assign our observed σ anisotropy to the fluorines at the (2)-sites, the surroundings of the fluorines at the (1)-site appearing quasiisotropic. Furthermore the isotropic chemical shift of the two sites must be almost the same, since in CRAMPS only one peak is found within the limits of the resolution (2ppm).

CuF_2 is an antiferromagnetic compound being paramagnetic at room temperature. The observed line width is too large to infer any structural information from the spin echo lineshape. To the knowledge of the authors the only published NMR on CuF_2 has been in the region of the Neel temperature and below, in zero-field.[29]

In spite of a careful search for fluorine incorporated in the 1-2-3-type superconductors, no indication of a positively shifted

fluorine signal, nor any signal of residual starting material of the preparation (YOF, EuOF, YF_3) therein was found. The present results indicate that the only fluorine-signals found in the compounds "$RBa_2Cu_3O_{7-x}F_x$" were small amounts of BaF_2, for R = Y: 5.10^{-1}, for R = Eu: ~ 2.10^{-1} mol(BaF_2)/(1 mol host).[4] This is in agreement qualitatively with our semiquantitative X-Ray diffraction analysis. The quantity of F detected in BaF_2 is 25 times or 8 times the minimum amount of F detectable for R = Y or Eu, respectively, under the present experimental conditions. These detection limits are predicated upon detectability in the superconductor (in the normal state) being the same as in the insulators and in Ag_2F studied in this work.

CONCLUSION

No detectable fluorine is incorporated into crystal structures of superconductors. Only F signal detected is from BaF_2 as an impurity. Two nonequivalent F's in YF_3 have the same isotropic chemical shifts.

ACKNOWLEDGEMENT

Enlightening discussions with the staff members of the Physics and Chemistry Departments and Ames Laboratories of Iowa State University are fully appreciated: on crystallographic questions with Dr. L. Miller, on clarification in Knight-Shift work with Dr. B. Harmon. Thanks for some experimental support are also due to Dr. M. S. Prusky and mostly to Dr. Vinco Rutar. Dr. R. E. McCarley and M. Close were of great help with their advice on the chemistry of silver fluoride and silver subfluoride and with their permission to use part of their equipment. H. L. thanks Dr. B. C. Gerstein for his kind hospitality during this work.

REFERENCES

1. H. H. Wang et al., Inorg. Chem. **27**, 5 (1988).
2. P. K. Davies et al., Solid State Commun. **64**(12), 1441 (1987).
3. T. A. Vanderah et al., Mater. Res. Bull. **24**, 121 (1989).
4. D. White, C. E. Lee et al., University of Pennsylvania, Philadephia, PA 19104. Abstract for 29th Experimental Nuclear Magnetic Resonance Spectroscopy Conference, Rochester, New York, April 17-21 (1988).
5. S. R. Ovshinsky et al., Phys. Rev. Lett. **58**(24), 2579 (1987).
6. Christopher Caretsopoulos, H. C. Lee et al., Phys. Rev. **B39**, 781 (1984).
7. R. Hilsch et al., Naturwissenschaften **44**, 463 (1957).
8. H. Nishihara, I. Shirotani, N. Inoue, Physica **105B**, 107 (1981) and J. Phys. Soc. Jpn. **48**(6), 1057 (1980).
9. D. K. Hindermann et al., J. Magn. Reson. **1**, 479 (1969).
10. R. W. Vaughan, D. D. Elleman et al., J. Chem. Phys. **57**, 5883 (1972).
11. D. P. Burum, D. D. Ellmann et al, J. Chem. Phys. **68**, 1164 (1978).
12. J. H. Clark et al., J. Chem. Soc. Chem. Commun. **No 1-12**, 657 (1986).
13. L. M. Avkhutsky, S. A. Polishuk, S. P. Gabuda, Sib. Chem. J. **4**, 455 (1968)(Engl. Transl. of: Izv. Sib. Otd. Akad. Nauk SSSR, Ser. Khim. Nauk **4**, 128 (July-Aug. 1968)).
14. S. P. Gabuda, S.V. Zemskov, J. Struct. Chem. **3**, 379

(1987)(Engl. Transl. of: Zh. Strukt. Khim. **28**, 56 (1987)).

15. D. C. Harris, T.A. Hewston, J. Solid State Chem. **69**, 182 (1987).
16. Lee Poyer et al., "Inorganic Syntheses", vol. V, pp. 18, McGraw Hill Book Co. Inc. New York 1957.
17. Joint Committee on Powder Diffraction Standards(JCPDS), Microfiche: No. 17-325 (Ag_2F) (see also: Nat. Bur. Stand. Report 9086, April 1966).
18. R. A. Wind et al., J. Magn. Reson. **52**, 424 (1983).
19. B. C. Gerstein, Philos. Trans. R. Soc. London. **A299**, 521 (1981).
20. Annu. Rep. NMR Spectrosc. **10B**, 5 (1980).
21. Q. Won Choi, J. Am. Chem. Soc. **82**, 2686 (1960).
22. Gmelins Handbuch der anorganischen Chemie, 8. Auflage, Verlag Chemie 1971; Silber: Teil B1; 5.3 Silberfluorid AgF, P.P. 297 ff.
23. L. M. Avkhutsky et al., Spectrosc. Lett. **2**(3), 75 (1969).
24. R. E. Connick, R. E. Poulsen, J. Phys. Chem. **63**, 568 (1959).
25. W. G. Ralph, "Crystal Structures", Second Edition Vol.1, pp. 268, John Wiley, New York 1962.
26. Int. Tables X-Ray Crystallogra, pp. 272, The Kynoch Press, Birmingham, England 1952.
27. Y. N. Mosckvinch, V. M. Buznik et al., Sov. Phys. Crystallogr. **23**(2), 232-234 (1978) (Engl. Transl. of Kristallografiya **23**, 416 (1978).

28. W. G. Raiph Wyckoff "Crystal Structures", Second Edition Vol. 2, pp. 58, John Wiley, New York 1962.

29. T. J. Bastow et al., Solid State Commun. **39**, 325 (1981).

30. Y. V. Gagarinskii, S. P. Gabuda et al., Sib. Chem. J. **1**, 82 (1968) (Engl. Transl.)

31. L. M. Avkhutsky et al., S. P. Gabuda, Dokl. Akad. Nauk SSSR (Engl. Transl.) **188**(6), 1285 (1968).

32. Y. V. Gagarinskii, S. P. Gabuda, J. Struct. Chem. (Engl. Transl.) **11**(5), 897 (1970).

Table 1: ^{19}F chemical shifts and linewidths in δ-scale relative to C_6F_6

Compounds	Single pulse					Spin-echo		Multipulse decoupling (MPD)			
	Static				MAS			Static			CRAMPS
	Peak center	$\delta_{\perp}$ ($K_{\perp}$)	$\delta_{\parallel}$ ($K_{\parallel}$)	Line width	$\bar{\sigma}$	Peak center	Line width	σ_{11}	σ_{22}	σ_{33}	$\bar{\sigma}$
Ag_2F	189±5	170	260	68	197±2						195±2
AgF (a) AgF (b)	-153±3 -145±3			71 75	-149±1			-150±1	-150±1	-150±1	
$AgF(H_2O)_x$ (x=2?)	40±2			74	37±2			(c)			
BaF_2	157±3			82	152±1			152±1	152±1	152±1	152±1
YOF	84±5	112±5	37±5	114	83±3			107±3	107±3	37±3	84±2
EuOF						460±20	800 (g)				
YF_3	103±15			183	(d)			140±3	108±3	82±3	111±2
CuF_2						60±10	290 (g)				
KF (e)	37±3			49				35±1	35±1	35±1	
KF (f) (Solution 35g/100ml	49±1										

Table 1: Continued

Compounds	Figure, see captions	Previous reported data		
Ag_2F	(1), (2)	139±25 [j]		
AgF [a] AgF [b]	(3), (4)	-90±25 [h]	-84±5 [i]	-153±5 [k], -174±5 [l] -154±5
$AgF(H_2O)_x$ (x=2?)	(3)	38±5 [m]		
BaF_2	(5)	154±1 [n]	153.5±1 [o]	135±8 [p], 116±20 [q]
YOF	(6)	56±20 [r]		
EuOF	(7)			
YF_3	(8)	86±20 [s]		
CuF_2	(9)			
KF [e]		37±1 [n]	40±3 [t,u]	
KF [f] (Solution 35g/100ml		38±3 [t,u] (dil.) 37±3 (3M/L)		45±3 [t,u] (dil.) 43±3 (14M/L)

Index to the table

(a) Before drying, as delivered and handled under dry N_2 gas; Shielded against light.

(b) After 24h of drying at 140°C, under vacuum ($3X10^{-2}$torr).

(c) Not possible to remove H•••F coupling of water.

(d) Resolution of peaks with MAS not possible.

(e) $KF•2H_2O$ dried at 150°C.

(f) δ is independent of concentration within the range 5-35% gKF/100ml solution (0.9-6M/L; secondary reference for Ag_2F and AgF).

(g) Halfwith of Spin-Echo-Envelope obtained by appropriate frequency variation.

(h) (8, 21) wherein error values are cited.

(i) (30)

(j) (21)

(K) (23, 31), error values are cited.

(l) The fist data is cited in(14), the second is taken from fig. 1 in (14).

(m) (24) AgF in 1 molar aqueous solution; δ-shift converted from F_2-to C_6F_6-scale.

(n) (10)

(o) (11)

(p) (23)

(q) (32)

(r) Are there pairs of fluorine in trigonal YOF?(27).

(s) (23, 32)

(s) (23, 32)

(t) (12) KF dried at >100°C; MAS at 3KHz; Shift values converted from $CFCl_3$-to C_6F_6-scale with $\delta(CFCl_3)-\delta(C_6F_6)=162.9$ppm (20).

(u) (24) Shift values converted F_2-to C_6F_6-scale with $\delta(F_2)-\delta(C_6F_6)=585.8$ppm (20); see also remarks under (1); all converted shift values suffer from this transformation and are therefore subject to an error.

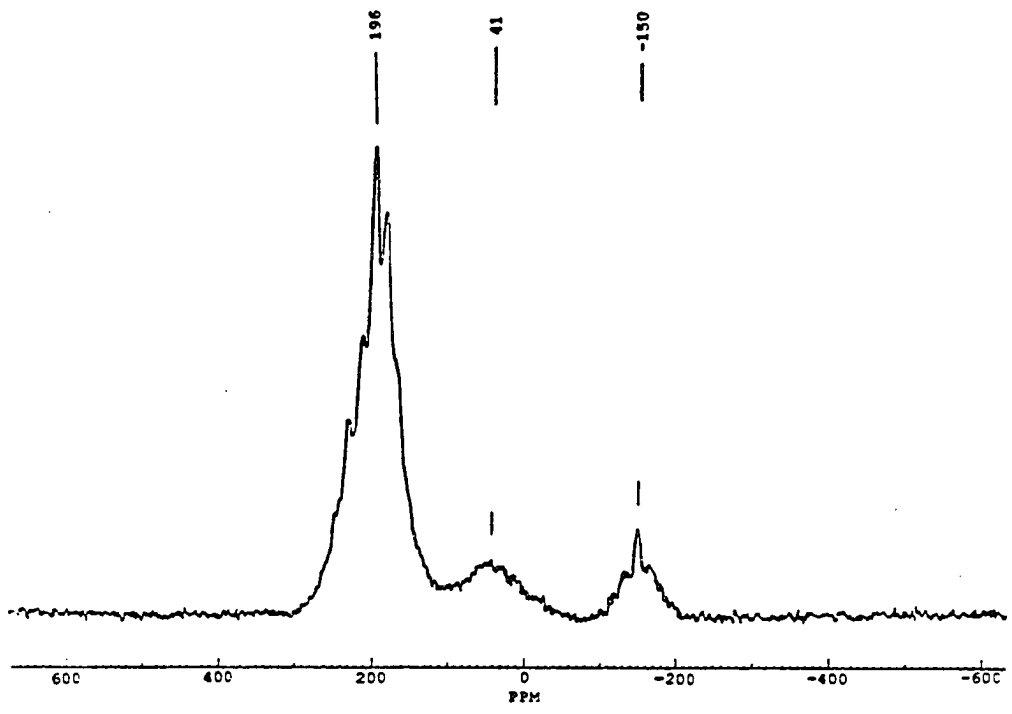

Figure 1: Ag_2F, δ~196ppm, with MAS. The sample still contains small amounts of $AgF \bullet (H_2O)_x$, δ~41ppm, and AgF, δ~-150ppm, after preparation.

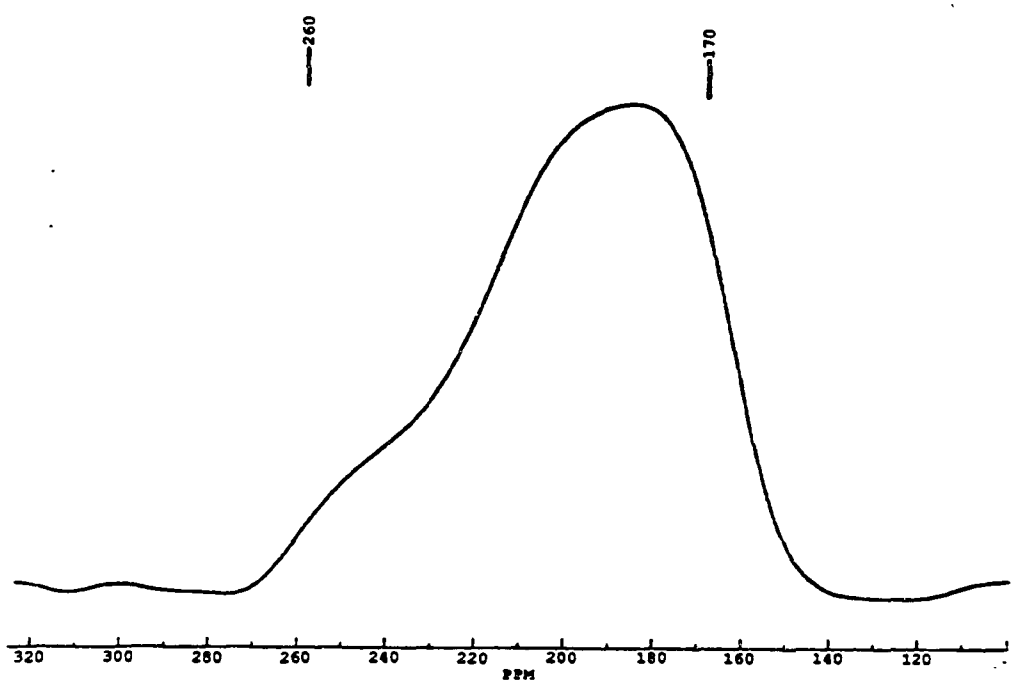

Figure 2: Anisotropic, static line pattern of the Knight-shifted Ag_2F, with $K_{||}$ ~260±5ppm, $K_{\perp}$~170±3ppm.

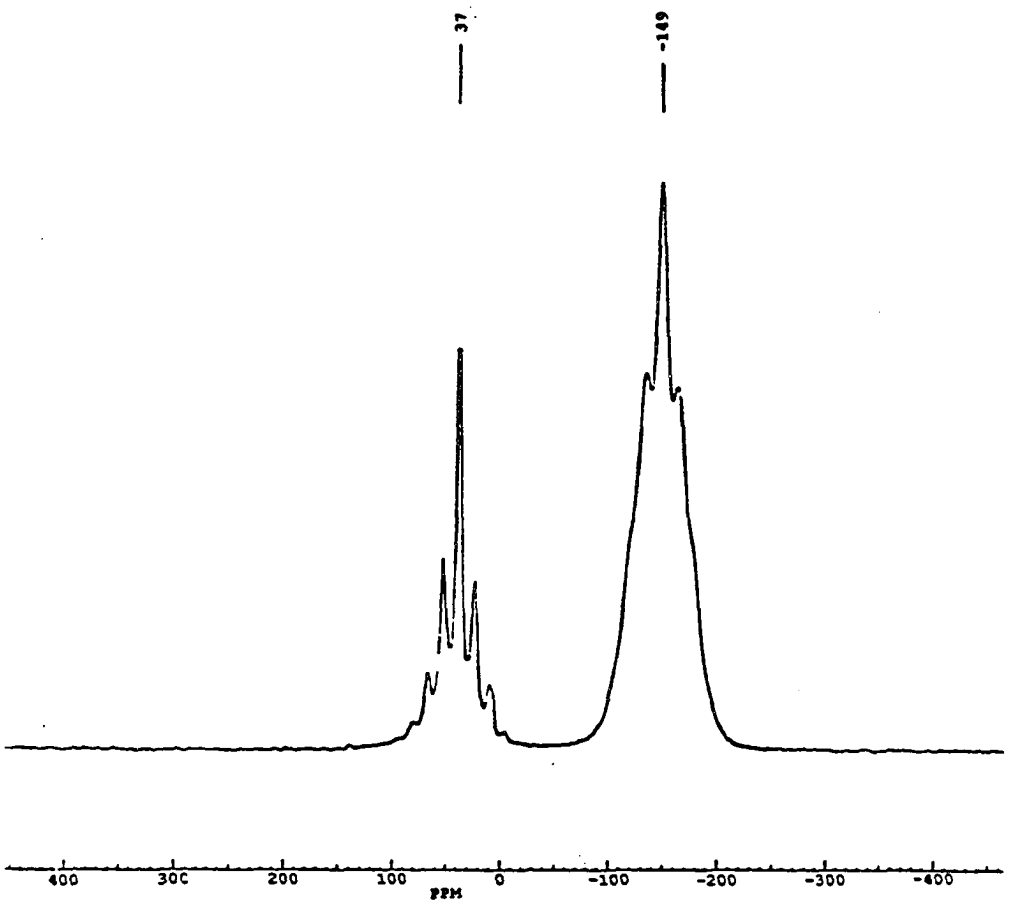

Figure 3: AgF, δ~-149ppm, "impurity" $AgF\bullet(H_2O)_x$, δ~37ppm, with MAS, before drying the sample.

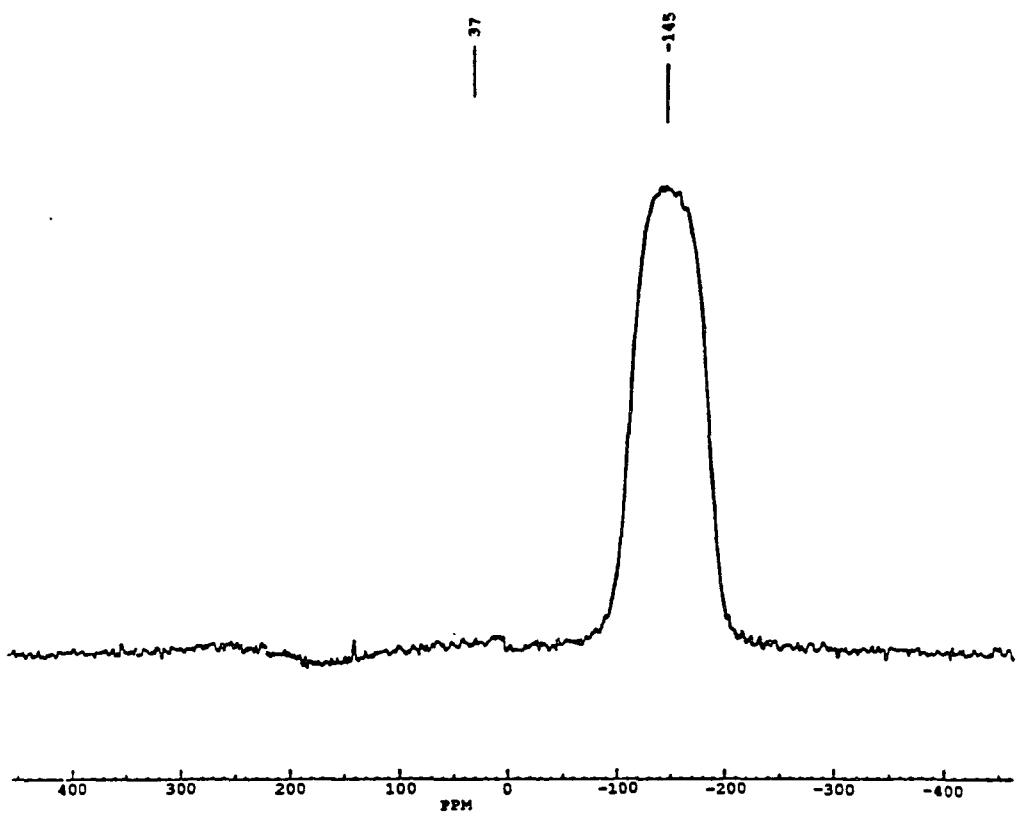

Figure 4: Static peak of AgF, δ~-145ppm, after drying the sample shown in figure 3; the peak at δ~37 ppm has disappeared.

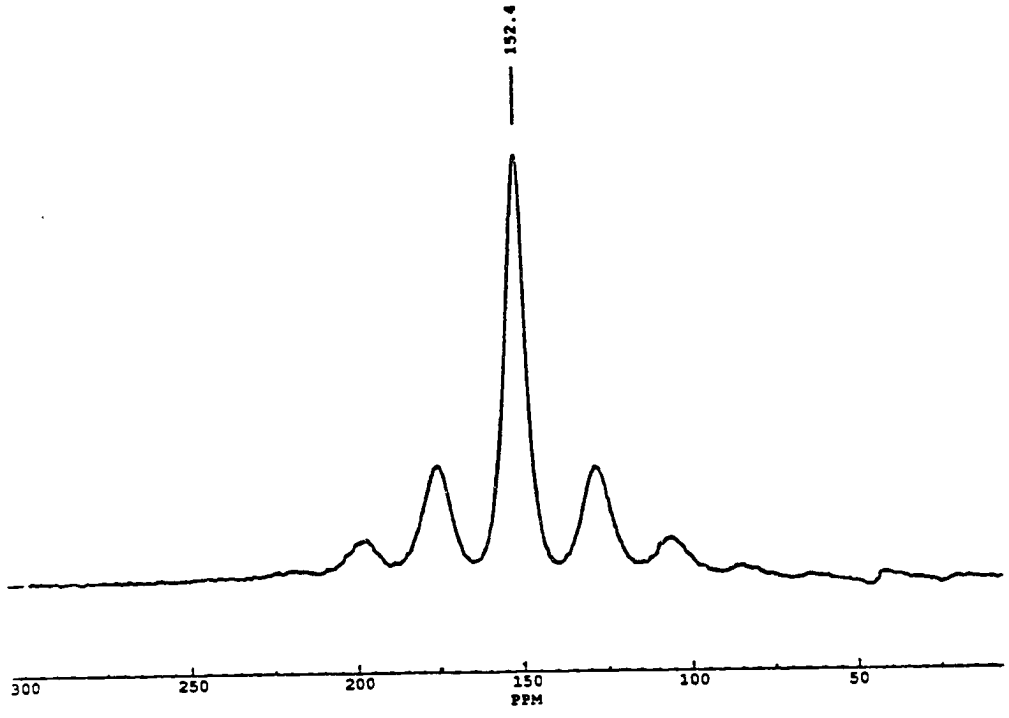

Figure 5: BaF_2, δ~152ppm, with MAS and ~6.3 KHz spinning frequency.

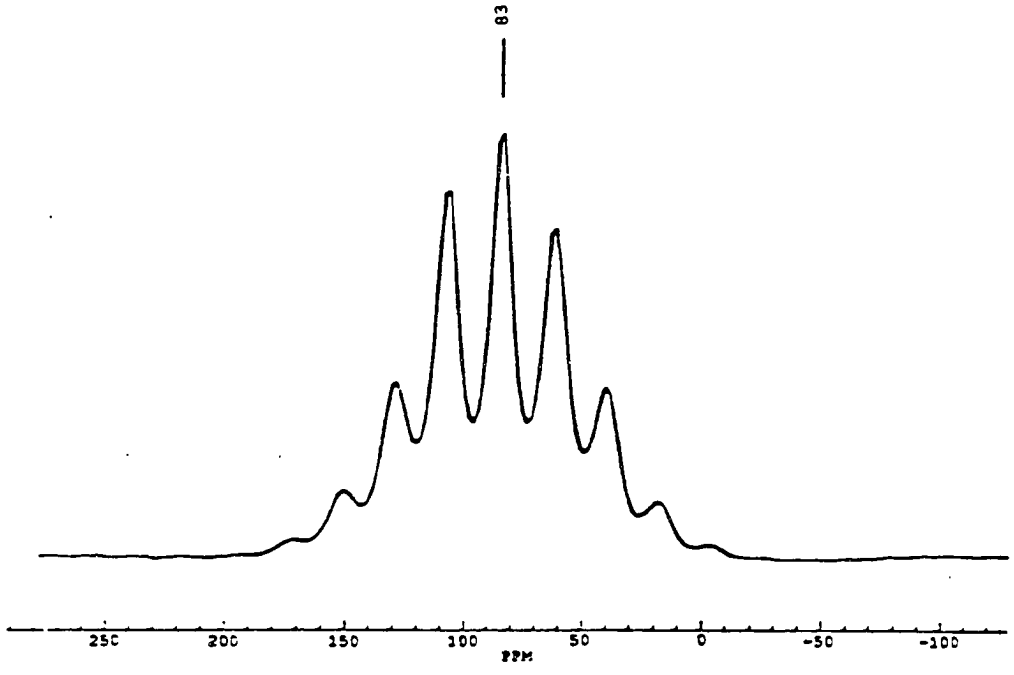

Figure 6: YOF, δ~83ppm, with MAS.

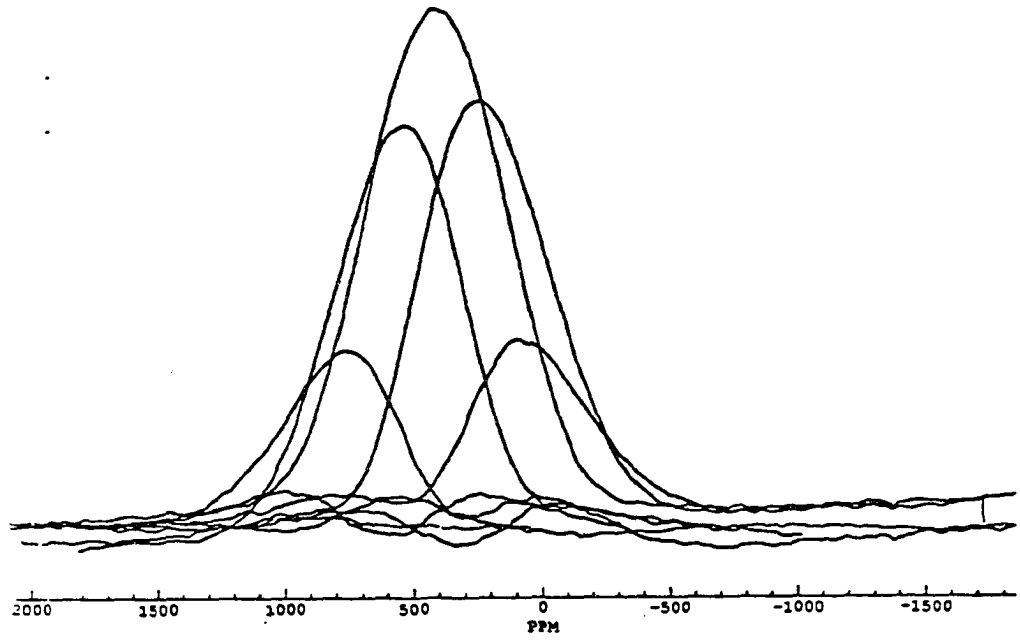

Figure 7: EuOF with Static Spin-Echo Mapping.

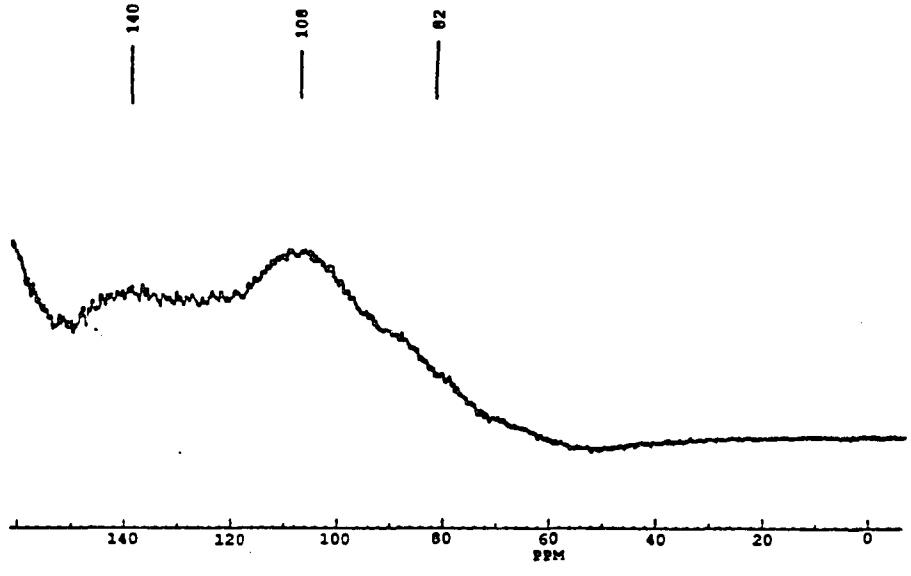

Figure 8: Static MPD of YF_3; 3 peaks at σ_{11}~140ppm, σ_{22}~108, σ_{33}~82ppm.

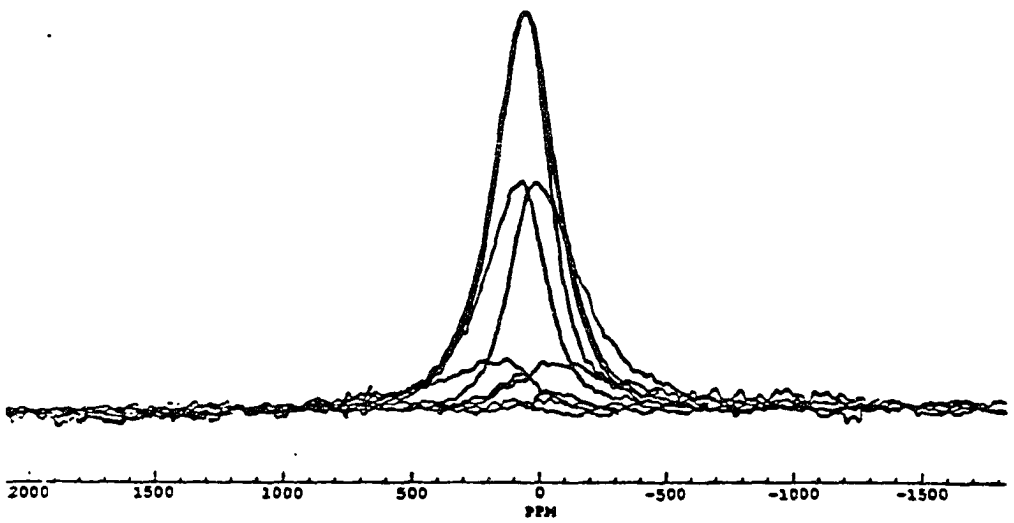

Figure 9: CuF_2, δ~60ppm, with Static Spin-Echo Mapping.

PART II. NMR STUDY OF LOCAL COORDINATION IN AMORPHOUS CARBON

NMR study of local coordination in amorphous carbon

Hongjun Pan, M. Pruski, and B. C. Gerstein

Institute for Physical Research and Technology

and

Department of Chemistry, Iowa State University

Ames, Iowa 50011

and

Fang Li and Jeffrey S. Lannin

Department of Physics, Pennsylvania State university

University Park, PA 16802

The authors research is supported by the Division of Basic Energy Science of the Department of Energy under contract No. W-7405-Eng-82.

ABSTRACT

Amorphous carbon has been studied by ^{13}C and ^{1}H NMR with techniques of static single excitation, magic angle spinning and CP/MAS. A spin-lattice relaxation time of 0.7s was obtained by progressive saturation method. Two different components which were resolved using the tensor fitting routine with Gaussian broadening functions are clearly seen in the spectrum of static sample. The downfield component corresponds to sp^2-like carbons which comprise 93.6% of the total signal and has an axially symmetric shift tensor with $\sigma_{||}$ = -28 ppm, $\sigma_{\perp}$ = 209 ppm and $\bar{\sigma}$ = 130 ppm. The upfield component corresponds to sp^3-like carbons which comprise 6.4% of total signal and has a symmetric shift tensor with $\bar{\sigma}$=62 ppm. The concentration of the dangling bonds is about $2X10^{20}/cm^3$. About two thirds of carbons are not seen in the static measurement because of high concentration of unpaired electrons leading to severe inhomogeneous line broadening. Those carbons are detected by magic angle spinning method in which sidebands spread over a range of 2000 ppm with the first moment located at 130(±5ppm). The upper limit of the fraction of hydrogenated carbons is 1.5%.

INTRODUCTION

Amorphous carbon as a material has been a subject of interest for a number of years.[1-13] Amorphous carbon is a type of semiconductor, mechanically hard, and semitransparent to visible light. It can be made by evaporation[2-4] or sputtering.[5-7] There are two types of amorphous carbon: hydrogenated and unhydrogenated. The unhydrogenated amorphous carbon has a small optical gap and a relatively high electrical conductivity;[5] the dangling bond density is also relatively high.[8] The hydrogenated amorphous carbon, in contrast, has a larger optical gap, low electrical conductivity and low dangling bond density.[6] Several models have been proposed to describe the structure and physical properties.[7,9-13] These studies differ from more schematic models of a-c which presume local structures that are graphite-like, i.e. systems with connected planar hexagonal rings. New experimental studies of the radial distribution function (rdf) of well characterized a-c films have demonstrated that the fundamental models are more correct in not exhibiting ordered hexagonal ring structures. While these hexagonal units appear to be present in certain nanocrystalline forms of C, including glassy C, their order is not consistent with the observed rdf of a-c.

The experimental rdf of a-c also demonstrates, as did earlier studies, that the average coordination number of C exceeds 3. The form of the rdf precluded, however, an accurate estimate of the fraction of 3-fold, sp^2 and 4-fold, sp^3 type sites. Information

about the fraction of 3-fold to 4-fold sites is of importance both for comparison with theoretical models as well as for estimating the relative structural disorder in bond distances and angles for each site. The rdf of a-c suggests, for example, that bond length fluctuations of 3-fold sites are substantially greater than those of a-Si and a-Ge systems with predominant 4-fold coordination. While this radial disorder is qualitatively consistent with a molecular dynamics model for a-c, certain aspects of the radial distribution differ from this theory. Additional information relevant to the properties and structural topology of a-c clearly require an improved estimate of the fraction of 4-fold sites.

One means of obtaining quantitative information about the fraction of 3-fold to 4-fold sites involves the use of NMR. Although it had been suggested that substantial H may be required to obtain appropriate relaxation times, it appears that the primary experimental limitation has been the preparation of a thin film sample of sufficient size to contain enough ^{13}C at natural abundance to be detectable by NMR. In the present study a combination of static, magic angle spinning and CP/MAS NMR yields ~6.5% 4-fold bonding. This value is below that estimated by detailed theoretical structure studies. The results thus emphasize that the electronic and vibrational properties of a-c are primarily determined by distorted 3-fold environments.

EXPERIMENTS

Amorphous carbon was prepared by rf sputtering on a 99.99% pure graphite target in a high vacuum system of base pressure $1x10^{-7}$ Torr. A 5" diameter cathode was sputtered at a power of 400 Watts at an Ar pressure of 8 mTorr. Substrates of Cu were placed in good thermal contact with a liquid nitrogen cooled plate to prevent film ordering due to heating. Such ordering is observed in the Raman spectra of films deposited on uncooled substrates as two distinct microcrystalline peaks. In contrast, a-c studied here exhibits a very broad high frequency band as well as additional low frequency scattering. Amorphous carbon films were removed from the substrate by using dilute HCl acid and cleaned thoroughly in deionized water. RDF measurements on this sample yielded a network density 1.08 times that of graphite. A macroscopic density 0.89 times that of graphite, in contrast, is due to film microporosity.

Because the sample was prepared without the deliberate introduction of hydrogen, most carbons are not hydrogenated, and one can expect that the sample has a high density of dangling bonds (or radicals). The paramagnetic interaction with the single electrons of those dangling bonds and the chemical shift interaction will dominate the nuclear spin-spin and the spin-lattice relaxation. The amorphous carbon in the studies reported here was probed using several transient techniques in NMR including single pulse static and MAS experiments on ^{13}C and ^{1}H, and cross-polarization with magic angle spinning (CP/MAS), using two

homebuilt spectrometers operating at 220 MHz and 100 MHz for ^{1}H (55.4 MHz and 25.15 MHz for ^{13}C), respectively. All NMR experiments were performed at room temperature. Single pulse excitation of ^{13}C was performed at 55.4 MHz using a static sample (100 mg) to extract the principal components of the chemical shift tensors and the fractional ratio of the components in different chemical environments. In this experiment, a 5 Ω resistor was connected in series with the resonance coil which reduced the recovery time of the spectrometer to 2 μs after the 7 μs π/2 pulse.

Residual hydrogen content of the sample was examined by ^{1}H NMR at the resonant frequency of 220 MHz. Both evacuated (at 90°C and 10^{-6} Torr for five hours) and unevacuated samples were measured to discriminate between protons in weakly adsorbed compounds such as water and hydrogens bonded to the amorphous carbon. The 90° pulse length was 3 μs. The recovery time was 3 μs after the pulse. A CP/MAS spectrum of ^{13}C was obtained to examine hydrogenated amorphous carbons at a frequency of 25 MHz for ^{13}C using a spinning speed of 4.4KHz and a proton B_1 field of 50 KHz for cross-polarization and decoupling. 32 mg of samples were used in MAS and CP/MAS experiments. Throughout this work, all resonance line positions were determinated with respect to tetramethylsilane (TMS). The δ scale is used with positive numbers being downfield. The unpaired electron spin concentration was determined by comparison of ESR intensities of the amorphous carbon with that of a standard sample of DPPH.

RESULTS AND DISCUSSION

The spin-lattice relaxation time of 0.7s for ^{13}C was determined for amorphous carbon at a resonant frequency of 55.4 MHz. A progressive saturation method with the maximum delay of 60s between the scans was used in this experiment. The ^{13}C-^{13}C and ^{13}C-^{1}H dipole-dipole interactions are not expected to be important for relaxation because of the low abundance of ^{13}C nuclei and the relatively low (~1.5 at%) concentration of hydrogen in the sample. The observed value of T_1 indicates that dipolar interaction with unpaired electrons in dangling bonds dominates spin-lattice relaxation. ESR measurements yielded a concentration of unpaired electrons in the sample of $2X10^{20}/cm^3$. It is noted, that in the earlier study of unhydrogenated a-c by Jansen et al.,[6] T_1 of carbon was found to be sufficiently long to prohibit an acquisition of NMR spectra. However, in the latter study a concentration of unpaired electrons of only $10^{18}/cm^3$ was found. The relatively large concentration of dangling bonds observed in the samples studied in the present work is attributed to reduced atomic mobility on cooled surfaces as well as substantial plasma bombardment in the rf sputtering process.

Fig. 1 shows the static NMR spectrum of ^{13}C in amorphous carbon resulting from 60,000 free induction decays taken with a delay of 4s between the scans and at resonant frequency of 55.4 MHz. The broad spectrum of Fig. 1 can be described as a superposition of two

components: a downfield component representing "sp^2-like" carbons with a relatively large (200 ppm) chemical shift anisotropy, and a much less intense, upfield signal representing sp^3-like carbons. The MAS spectrum, taken at 25.12 MHZ (50,000 accumulations with a 4s delay) is given in Fig. 2. It is interesting to note that although magic angle spinning resulted in a reduction in linewidth by a factor of almost three, the "resolution" in the MAS spectrum is not significantly improved. The overlapping of the isotropic peaks corresponding to the two carbon fractions results from severe residual broadening presumably due to the interaction with unpaired electrons. Also, the distribution of bond length in amorphous carbon contributed to the broadening of the NMR line which could not be eliminated by MAS.

The spectra of Fig. 1 and Fig. 2 were used to estimate the sp^2/sp^3 ratio in the sample. The two components were resolved in Fig. 1 (dashed lines) using a tensor fitting routine with a Gaussian broadening of 2.8 KHz. The sp^2 component comprises 93.6(±1.5%) of the total signal, and could be well approximated using an axially symmetric shift tensor with $\sigma_{||}$ = -28 ppm, $\sigma_{\perp}$ = 209 ppm and $\bar{\sigma}$ = 130 ppm. The asymmetry of the tensor is higher than Resing's result for graphite with $\sigma_{||}$ = 0 ppm, $\sigma_{\perp}$ = 178 ppm and $\bar{\sigma}$ = 119 ppm but the isotropic chemical shift observed in the present work is close to that observed by Resing for graphite.[14] The shift due to a bulk susceptibility associated with $2X10^{23}/cm^3$ unpaired electron spins 1/2 would be 0.11 ppm downfield, so the difference of 11ppm between the present results and those for

graphite must be accounted for in terms contact shift or distortion relative to the highly ordered graphite structure. The direction of shifting (upfield for $\sigma_{||}$ and downfield for $\sigma_{\perp}$) indicates that the electron density perpendicular to the sp^2 plane is higher than that of graphite and the electron density in the sp^2 plane is lower than that of graphite. The second component in the spectrum of Fig. 1 may be interpreted in terms of a symmetric tensor with a line broadening of ~2.7 KHz, and an isotropic chemical shift $\bar{\sigma}$ of 62 ppm representing "sp^3-like" carbons. The sp^3 carbon signal comprises 6.4(±1.5)% of the total intensity. The NMR data are consistent with that of neutron diffraction experiments which indicated that there is a small fraction of four-fold bonds present in this sample.[16]

Note that the spectrum presented in Fig. 1 does not represent all carbons in the sample. Spin counting, which was performed by integrating the intensity of ^{13}C spectrum from Fig. 1, compensating the result for the loss due to deadtime, and comparing it with that of a reference sample, showed that only 28(±5)% of the total carbons in the sample were detected by NMR. The presence of unpaired electrons is assumed to be the primary reason for the loss of intensity of the ^{13}C nuclei in the static experiment. The resonances of those nuclei for which the electron-nuclear dipolar interaction is large compared to the width of the static NMR spectrum contributed to the broad baseline spreading far beyond the range presented in Fig. 1 and could not be distinguished in this experiment. Also, Fig. 1 does not include the ~1.5% of carbons which form C-H bonds(discussed later in this work).

The results of spin counting do not apply to the MAS spectrum of Fig. 2. An interesting feature of this spectrum is the presence of spinning sidebands(see the inset in Fig. 2) which spread over a range of more than 2000 ppm (50 KHz). The only inhomogeneous interaction which could give rise to such broad pattern of sidebands is the coupling between ^{13}C nuclei and unpaired electrons(at a resonant frequency of 25.2 MHz a spinning speed of 5KHz eliminates spinning sidebands due to chemical shift anisotropy). As demonstrated by Nayeem et al.,[15] the powder pattern lineshape of a static paramagnetic solid is affected by the anisotropic part of the dipolar interaction between an electron and a nucleus. Even in the presence of several unpaired electrons around a given nucleus, the net inhomogeneous interaction responsible for the occurrence of sidebands in the MAS spectra is formally equivalent to that of a chemical shift tensor. It is, therefore, concluded that the sidebands represent most of those carbons which were 'invisible' in the static spectrum of Fig. 1. Since the acquisition of a spectrum with a considerably improved S/N was not possible due to the projected length of the experiment, the sidebands were not used to extract information concerning chemical functionalities of carbon involved. However, a computer analysis of the central peak allowed the estimate that the fraction of sp^2-like component is 93.1% and the fraction of sp^3-like component is 6.9% with the isotropic peaks located at 130 ppm and 65 ppm, respectively, in agreement with the results derived from analysis of the static spectrum. Our analysis showed that the

integration of the intensity of the signal(including all sidebands) from carbons close to unpaired electrons(invisible in Fig. 1) is 2.9 times that of signal from the carbons visible in Fig. 1. This result is very close to that of the spin counting experiment. The first moment is located at 130(±5) ppm which indicates that the major portion of those carbons invisible in static measurement has sp^2 coordination, this is consistent with the result of the static spectrum.

Quantitative measurements of proton content were performed by comparison of NMR spectral areas of both evacuated and unevacuated samples with that of reference. The result indicates that the sample consists of ~2.2% at% protons. Only half of those protons remained after evacuation. Neutron diffraction gives about 3 at% protons in the unevacuated sample.[16] The difference may be due to the high density of radicals which cause some loss of proton signal relaxation to paramagnetic centers. Assuming that neutron diffraction data reflects all protons in sample, an upper limit for the fraction of hydrogenated carbons is 1.5%.

Fig. 3 represents the CP/MAS spectrum of amorphous carbon resulting from 200,000 accumulations taken with a delay of 2 s and a contact time of 1ms. Since in the CP experiment, the polarization of ^{13}C nuclei is achieved indirectly through the dipolar interaction with the neighboring protons, the spectrum from Fig. 3 represents only those ^{13}C spins which are in the vicinity of protons (not more than 2-3 bond distances away). This is to say that the spectrum in Fig. 3 represents at most 1.5% of the carbons

in the sample. The hydrogenated carbons were formed during the sample preparation, probably due to the residual H_2O or other proton containing compounds in the vacuum chamber. It is seen that even under the high resolution condition of CP/MAS and proton decoupling a severe line broadening is observed. The main feature in the spectrum centered at ~140 ppm represents sp^2-like hydrogenated carbons which is close to Bustillo's CP/MAS result (145 ppm) for sp^2 hydrogenated carbons.[17] The spectrum in the region of 40 ppm to 120ppm is relatively flat suggesting that in addition to the sp^2 C-H bonds there exist some sp^3-like C-H bonds (resonances at 40-50 ppm) and a variety of intermediate C-H bonds. This could be the result of the structural distortion of sp^2 and sp^3 hybridizations in those C-H bonds. Such structure distortion will cause a distribution of ^{13}C resonances. Again, it should be noted that the presence of paramagnetic centers associated with dangling bonds in the sample may cause additional broadening of the resonance lines in the CP/MAS spectrum.

Note also that the resolution of the CP/MAS spectrum is not improved compared to the static spectrum of Fig. 1, which, as indicated earlier, could be well fitted by two chemical shift tensors. This observation may indicate that the bulk structures of "sp^2- and sp^3-like" carbons unattached to protons are rather well defined. In contrast, the C-H carbons, which are expected to be located at the edges of the amorphous carbon network, could exhibit more significant structural distortions. Since the dangling bonds are easily formed at the edges of the carbon network,[8] it is

reasonable to assume that those carbons which give sidebands in Fig. 2 are also adjacent to structural distortions, which either are directly connected or very close to the dangling bonds.

CONCLUSION

Two different components are observed in amorphous carbon with T_1 of 0.7 s by ^{13}C NMR. The downfield component corresponds to sp^2 structure which comprises 93.6% of sample and upfield component to the sp^3 structure which comprises 6.4% of the sample. The concentration of the unpaired electrons is about $2X10^{20}/cm^3$ which is responsible for the short T_1 and broadening of the spectra. Two thirds of carbons are not seen in the static measrement because of high concentration of unpaired electrons leading to severe inhomogeneous line broadening. Those carbons are detected by MAS experiment with sidebands spreading over a range of 2000ppm. The first moment located at 130(±5)ppm indicates that the major protion of those carbons has sp^2 coordination. The upper limit of the fraction of hydrogenated carbons is 1.5%.

REFERENCES

1. R. E. Franklin, Acta Cryst. **3**, 07(1950).

2. C. J. Adkins et al., Phil. Mag. **22**, 180(1970).

3. M. Morgram, Thin Solid Films **7**, 313(1971).

4. M. D. Blue and G. C. Daniellson, J. Appl. Phys. **28**, 583(1957).

5. J. J. Hauser, J. Non-Cryst. Solids, **23**, 21(1977).

6. F. Jansen, M. Machonikin, S. Kaphan, and S. Hark, J. Vac. Sci. Technol. **A3**(3), 605(1985).

7. S Kaphan, F. Jansen and M. Machonkin, Appl. Phys. Lett. **47**(7) 750(1985).

8. N. Wada, P. J. Gaczi, and A. S. Solin, J. Non-Cryst. Solids **35/36**, 543(1980).

9. J. Tersoff, Phys. Rev. Lett. **61**, 2879(1988).

10. G. Galli, R. M. Martin, R. Car and M. Parrinello, Phys. Rev. Lett. **62**, 555(1989).

11. D. Beeman, J, Silverman, R. Lynds and M. R. Anderson, Phys. Rev. **B30**, 870(1984).

12. J. Robertson, Adv. Phys. **35**, 317(1986).

13. E. P. O'Reilly, J. Non-Cryst. Solids, **97 & 98**, 1095(1987).

14. H. A. Resing and D. L. Vanderhart, Zeitschrift fur Physikalische Chemie Neue Folge, **151**, 137(1987).

15. A. Nayeem, J. Yesinowski, J. Chem. Phys. **89**(8), 4600(1988).

16. Fang Li, J. Lannin, Phys. Rev. Lett, **65**, 1905(1990).

17. K. C. Bustillo, M. A. Petrich and J. A. Reimer, Chem. Mater., **2**(2), 202(1990).

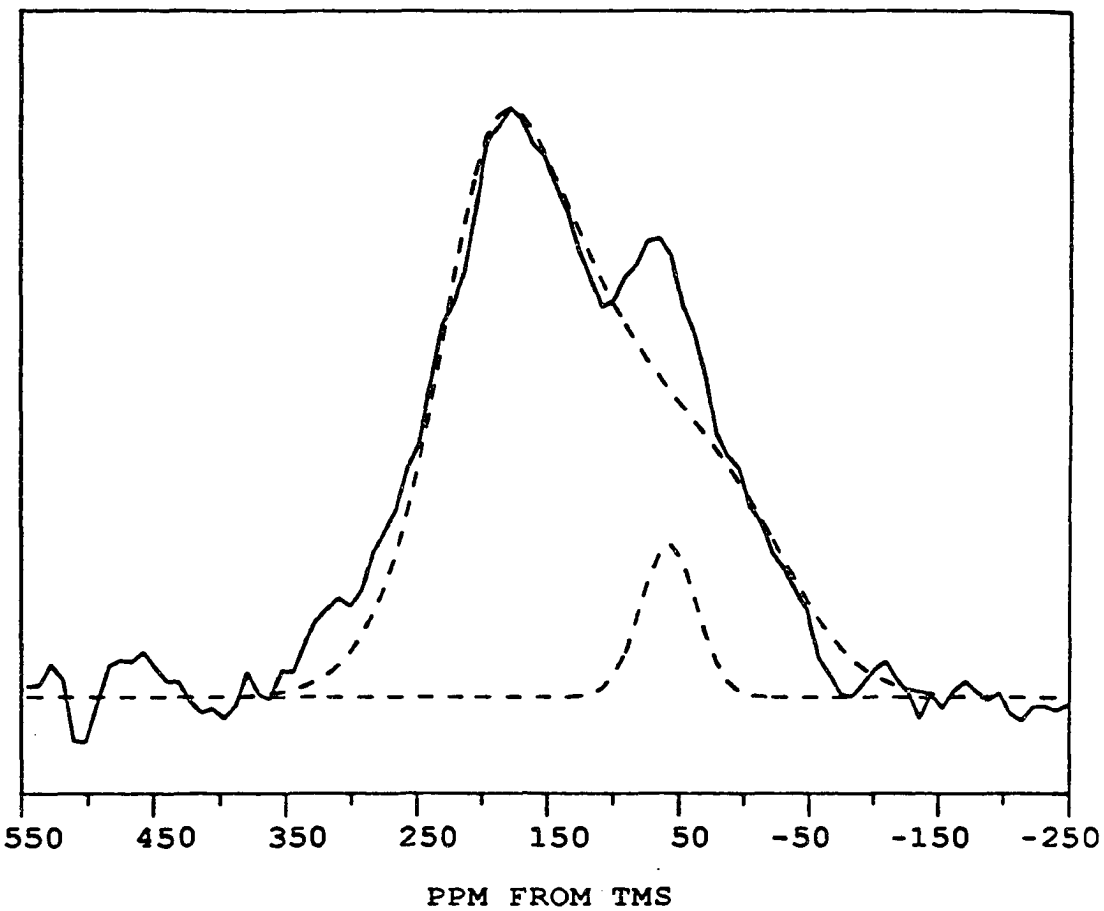

Figure 1: Static spectrum of ^{13}C in amorphous carbon

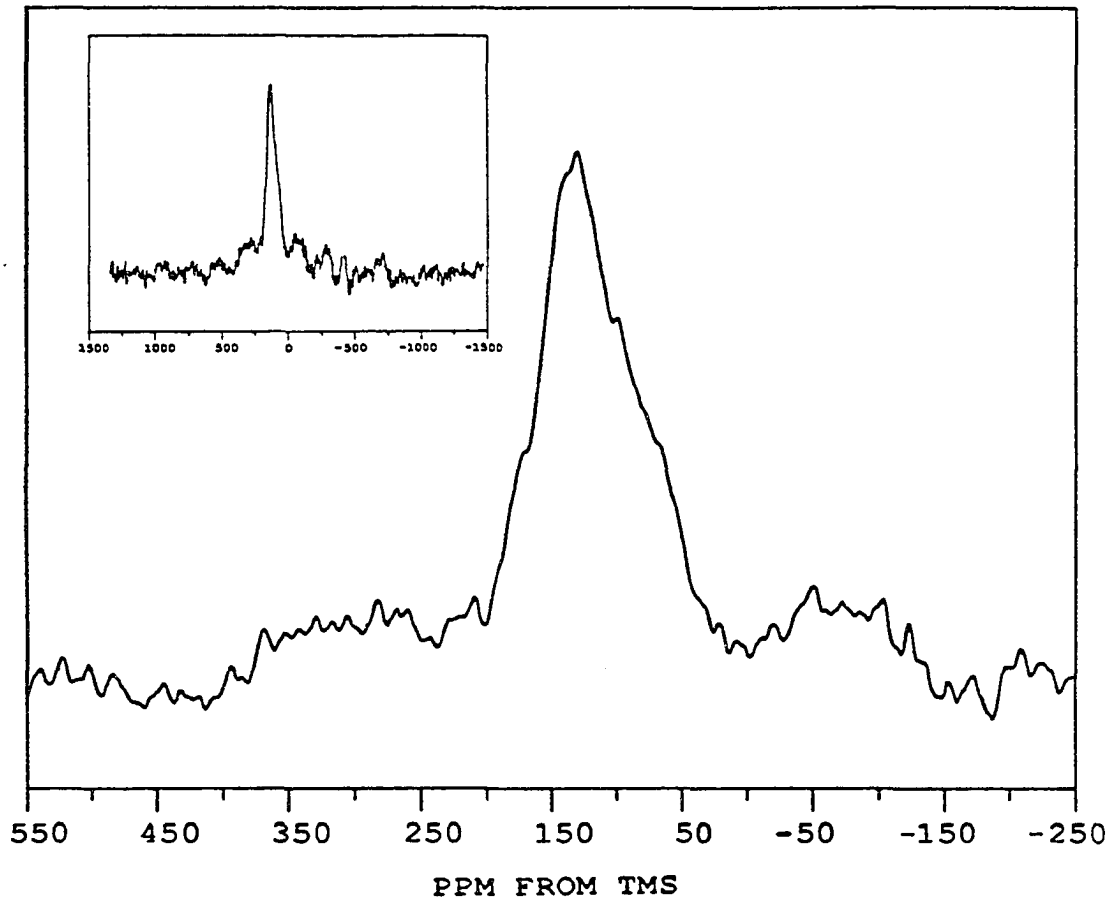

Figure 2: Magic anlge spinning spectrum of ^{13}C in amorphous carbon

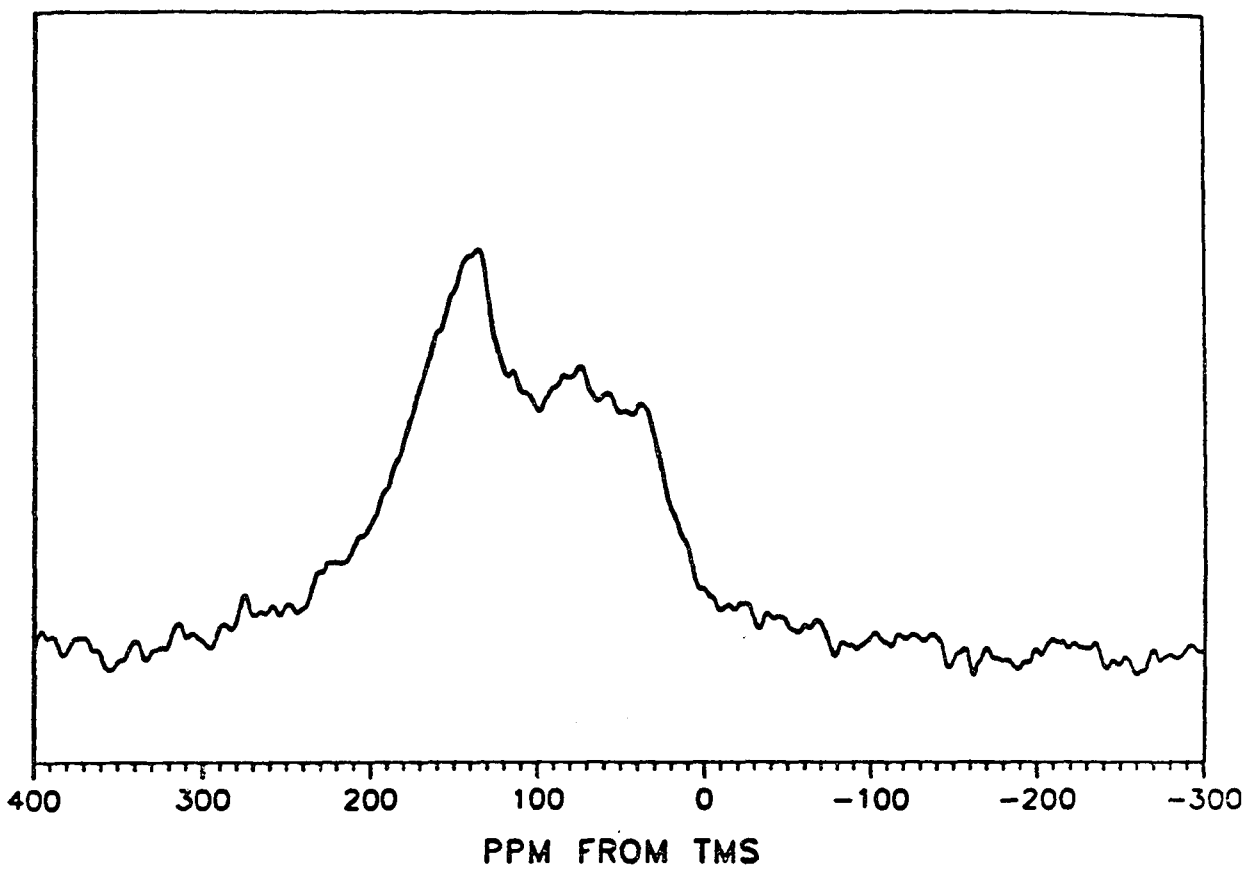

Figure 3: CP/MAS spectrum of ^{13}C in amorphous carbon

PART III: NMR OF ^{31}P IN $(VO)_2P_2O_7$ AS AN INTERNAL TEMPERATURE STANDARD IN HIGH TEMPERATURE NMR

NMR of ^{31}P in $(VO)_2P_2O_7$ as an internal temperature Standard in high temperature NMR

Hongjun Pan and B. C. Gerstein

Institute for Physical Research and Technology

And

Department of Chemistry, Iowa State University

Ames, IA 50011

This work was performed in the Ames Laboratory, operated for the US Department of Energy by Iowa State University, under Contract No.W-7405-Eng.82.

ABSTRACT

The temperature dependence of the chemical shift of ^{31}P in $(VO)_2P_2O_7$ has been studied. A Curie-Law type temperature dependence of the isotropic chemical shift was observed which can be used as an internal temperature standard in high temperature NMR.

INTRODUCTION

High temperature (to 700K) NMR experiments are desirable in modern NMR laboratories working with e.g. heterogeneous catalysis. One manner of heating is to bathe the sample in a flow of hot gas, but this has a disadvantage of extensive dewaring which is costly and complicates the experiment. Maresch and et al. overcame a good part of this difficulty by using radiofrequency irradiation of a platinum mirror on the NMR tube containing the sample,[1] such that the thickness of the mirror was well below the skin depth of the nucleus being irradiated, but of sufficient depth that eddy current heating was effective.

One problem in performing NMR experiments in such systems is that of measuring sample temperature. For temperatures below room temperature, Haw and co-workers have used the paramagnetic shift of ^{13}C in the carbonyl resonance of samarium acetate tetrahydrate.[2] The present note reports the use of such an idea in a compound which is suitable for temperature measurement at temperatures well above room temperature. Such a compound must meet the following requirements: (a) the NMR signal has a known temperature dependence, with slope, $d\delta/dT$ of sufficient magnitude to useful in detecting temperature increments to within a degree; (b) its NMR signal does not interfere with the NMR signal of the sample under investigation; (c) there is high NMR sensitivity; (d) the compound is thermodynamically stable in the temperature range under

consideration. We have found that the NMR of ^{31}P in paramagnetic $(VO)_2P_2O_7$ meets all above criteria.

EXPERIMENT

$(VO)_2P_2O_7$ was prepared by the high temperature reduction of β-$VOPO_4$.[3] β-$VOPO_4$ was placed in platinum lined quartz boats and placed in a quartz tube furnace. The quartz chamber was purged with oxygen free nitrogen (less than 5 ppm oxygen, Matheson) for 3 hours; this flow was maintained during the following heating stages. The chamber was then heated from 473K to 673K over 2 hours. After maintaining a temperature of 673K for 2 hours, the sample was heated to 1033K over 1 hour. The sample was held at this temperature for 36 hours then cooled to 573K over 9.2 hours and then to room temperature. This method of reducing β-$VOPO_4$ to $(VO)P_2O_7$ is documented by Bordes.[4]

^{31}P NMR measurements were performed in a Bruker MSL-300 operated at 121.5 MHz. H_3PO_4 (85%) is used as a reference. The sample was heated by blowing hot gas and the temperature was controlled within ±0.5°.

RESULT AND DISCUSSION

Fig. 1 shows the temperature dependence of isotropic chemical shift of ^{31}P in $(VO)_2P_2O_7$. The Curie-Law type temperature dependence of ^{31}P in this compound is observed with the relation

$$\delta = 414621/T + 1118.4 \qquad [1]$$

From [1], one can see that this sample has a well defined temperature dependence of chemical shift with sufficient magnitude of slope. ^{31}P has a natural abundance of 100% and resonates reasonably far from other commonly studied nuclei such as ^{13}C, ^{1}H, ^{19}F, ^{29}Si and ^{27}Al. $(VO)_2P_2O_7$ is thermodynamically stable up to 600K. So it is suitable as a internal temperature standard.

A single coil double resonance probe can be used for a single resonance study, with one channel tuned to ^{31}P to obtain the temperature and the other to the nucleus of interest. For double or triple resonance studies, a single coil triple or quadruple resonance configuration can be used.(5)

As a note of caution, $(VO)_2P_2O_7$ catalyzes the oxidation of C_4 hydrocarbons to maleic anhydride at temperatures near 500K, so if this compound is to be used as an internal temperature standard for NMR via the chemical shift of the ^{31}P in samples containing hyrocarbons near these temperatures it would best be used sealed in a thin walled quartz tube inserted into the sample in question.

CONCLUSION

The Curie-Law type temperature dependence of the chemical shift of ^{31}P in $(VO)_2P_2O_7$ can be used as a internal temperature standard in high temperature NMR.

REFERENCES

1. G. G. Maresch, R. D. Kendrick, and C .S. Yannoni, Rev. Sci. Instrum. **61**(1), 77 (1990).
2. James F. Haw, Analytical Chemistry, **60**, 559A(1988).
3. R. W. Wenig and G. L. Schrader, Ind. Eng. Chem. Fundam. **25**, 612(1986).
4. E. Bordes, Catalysis Today, **3**, 163(1988)
5. Robert A. Mckay, Dpt. of Chemistry, Washington Univ., St. Louis, MO, 63130, Poster WP 16 presented at the 31st Experimental NMR Conference, Asilomar, CA, April 1-5, 1990.

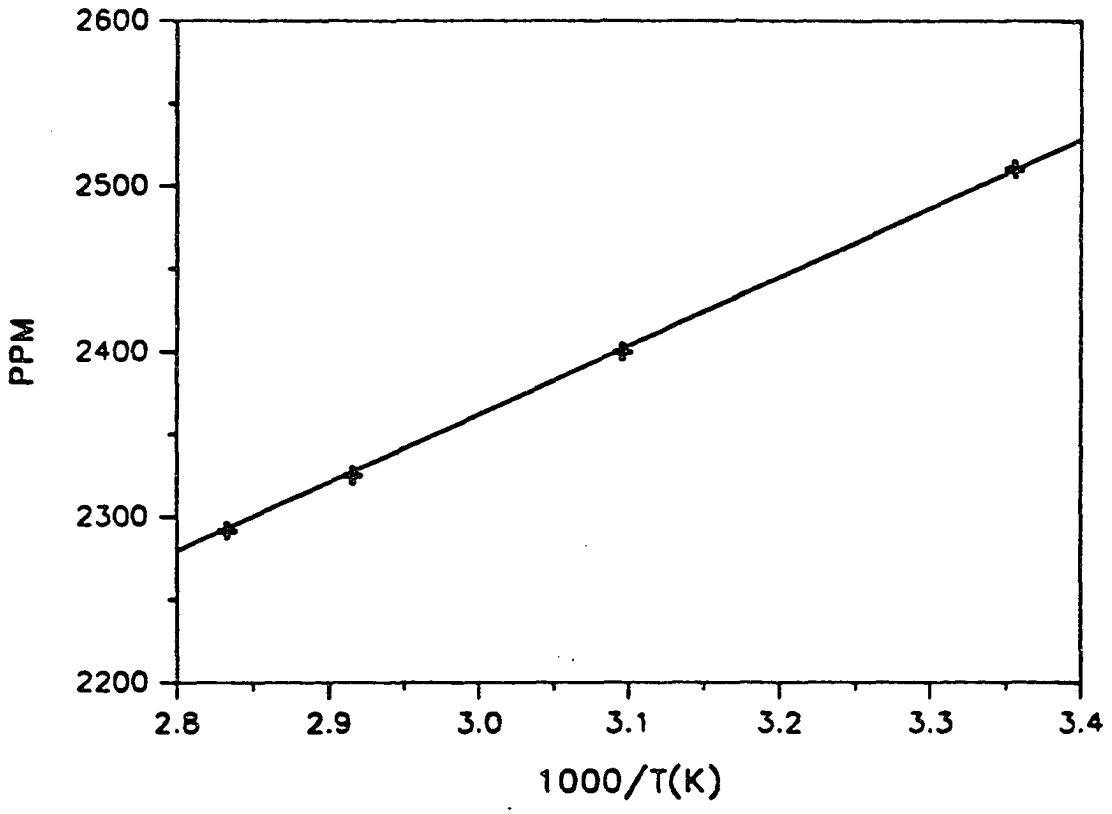

Figure 1: Temperature dependence of the chemical shift of ^{31}P in $(VO)_2P_2O_7$

PART IV: STABLE SYSTEM FOR MULTIPLE PULSE, MAGIC ANGLE SPINNING AND DYNAMIC ANGLE SPINNING NMR

Stable system for multiple pulse, magic angle spinning and Dynamic Angle Spinning NMR

Hongjun Pan, Bernard Gerstein, and Marek Pruski

Institute for Physical Research and Technology

And

Department of Chemistry, Iowa State University

Ames, Iowa 50011

The authors' research is supported by the Division of Basic Energy Science of the Department of Energy under contract No. W-7405-Eng-82.

ABSTRACT

A stable rotor-stator system is described that is suitable for NMR experiments of homonuclear decoupling, magic angle spinning and dynamic angle spinning. Speed to 16 KHz is achieved. The angle of rotation can be changed by 45° in 9 ms with no loss in rotation stability when spinning at normal speed of 10 KHz.

INTRODUCTION

The solid state NMR is dominated by anisotropies of chemical shifts, nuclear dipolar-dipolar interactions and quadrupolar interactions which make the NMR spectrum featureless. Modern transient NMR experiments for high resolution on solids[1-7] can require: (a) spinning of samples[8, 9] to rotational frequencies of order of 10 KHz,[10] (b) stability of spinning of order of 2Hz over periods of weeks in the case of long longitudinal relaxation times, (c) stability to rapid ($\leq$ 100 ms) changes in spinning angle, (d) uniformity of rf magnetic fields B_1 to better than 1% over 5-mm-diam sphere, (e) sufficiently compact dimensions to fit easily into a superconducting magnent with 51 mm bore. While there exist to our knowledge at least two commercially available NMR probes that meet some or all of these criteria,[11, 12] their construction is of ceramics such as alumina or zirconia that require specialized diamond tools for machining, and/or are relatively complicated in nature. Developing a stable rotor- stator system which can serve all above requirements with relative simple construction and easy machining is desirable. In the present work, a design of a new type of double bearing probe is described. This double bearing probe requiring relatively precise machining of polyimid type polymers was used first in this laboratory showing an advantage of increased stability and higher spinning rate in comparison with a single bearing probe. It can be used in the experiment of dynamic angle spinning.

REVIEW OF THE DEVELOPMENT OF SOLID STATE NMR

In an ensemble of nuclear spins of types I and S, the internal interactions affecting the nuclear spin energies are described by the Hamiltonian H_{int}:

$$H_{int} = H_{II} + H_{SS} + H_{IS} + H_Q + H_S + H_L \qquad [1]$$

H_{II} and H_{SS} represent homonuclear dipolar interactions among I spins and S spins respectively, H_{IS} is the heteronuclear dipolar interactions between I spins and S spins; H_Q is the quadrupole Hamiltonian of the I and S spins respectively; H_S contains all shielding Hamiltonians (chemical shift and Knight shift) of the I and S spins; H_L describes the spin lattice interaction. In fact, all those Hamiltonians can be expressed by irreducible spherical tensors as:[4]

$$H = \sum_{k=0}^{2} \sum_{q=-k}^{k} (-1)^q A_{kq} T_{k-q} \qquad [2]$$

where A_{kq} refers to spatial coordinates and T_{kq} to spin variables.

The NMR spectrum of a liquid consists of numberous sharp lines typically with linewidth due to magnetic field inhomogeneties or spin relaxation less than 1Hz.[13] The interaction Hamiltonian in a liquid sample is dominated by isotropic chemical shift and scalar spin-spin interactions. All possible anisotropic interactions, namely chemical shift anisotropy, dipole-dipole interaction,

quadrupole interaction etc. are averaged to zero due to the rapid isotropic molecular motion.

In the solid state, all these anisotropic interaction are retained and may be used to monitor the symmetry properties [Fig. 7] and the electronic state of the solid.[13] For ensembles of spin 1/2 systems (like ^{19}F and ^{1}H), the dipole-dipole interaction is the dominant interaction at ordinary magnetic field strengths (1-6 tesla). The result is in a more-or-less bell shaped, structureless line (Fig. 8a) from which very little information can be extracted about the local symmetry and other information. This led to the belief that NMR was useless for inferring detailed chemical information about solid samples in the early 50's.

In order to achieve the goal of high resolution NMR in solids, special techniques must be developed to manipulate the solid system and repress 'unwanted' interactions considerably and leave 'wanted' interactions more or less unaffected to extract useful information, because different interactions contain different information. The first breakthrough in solid state NMR to overcome this obstacle was made independently by E. R. Andrew et al.[14] in 1958 and by I. Lowe[8] in 1959 by using specimen rotation. In this method, the whole sample is rotated about an axis titled by the 'magic angle' $\theta_m = 54°44'8"$ which respect to the static field H_0. The efficiency of this method is shown in Fig. 8b. When the sample rotates at this angle at a frequency satisfying the condition $f_{rot} > \delta f_{dipolar}$, the average dipolar interaction vanishes, and the shielding anisotropies are also averaged to zero. The second breakthrough in

solid state NMR was made by J. S. Waugh and et. all[15] in 1968 by using four-pulse cycle and by P. Mansfield[16] in 1970 and W. K. Rhim and et. al.[17] in 1973 by using eight-pulse cycle to repress the homonuclear dipole-dipole interaction and obtain chemical shift information. Since then, multiple-pulse techniques have been developed for various purposes. Most samples of chemical interest contain many chemically nonequivalent species. Multiple pulse decoupling only removes the dipole-dipole interaction and is not sufficient for unique identification of shielding components because of the problem of overlapping tensors. Magic angle spinning can remove the anisotropies of the chemical shift. Combining multiple pulse decoupling with magic angle spinning will result in unique identification of isotropic shielding components of chemical nonequivalent species. This attempt was first made and experimentally achieved by B. C. Gerstein et. al. in 1977.[18] The high resolution NMR with 2ppm resolution become realistic in solid samples and the solid state NMR became an important tool in research to obtain isotropic chemical shifts of spin 1/2 nuclei in strongly homonuclear dipolar broadened solids.

There are many nuclei, namely, ^{13}C, ^{15}N etc. which can give valuable information about the electronic structure of molecules, especially the organic molecules which are most commonly studied. Because of their low natural abundance, small gyromagnetic ratio and coupling to abundant nuclei such as ^{1}H or ^{19}F, the NMR signals of the low abundant nuclei are broad and of low intensity. In order to detect these types of rare spins, a wealth of double resonance

techniques have been developed. The basic ideas were proposed by Hartman and Hahn in 1962,[19] from which different schemes are derived. Since the NMR signal of the rare spins is very weak, a gain in sensitivity can be obtained by utilizing the reservoir of abundant spins. This can be done in two ways: (i) by the indirect method,[19, 20] where the rare spins are detected via the abundant spins and (ii) by the direct method,[21] where the rare spins are polarized by the abundant spins. Although the indirect method is of higher sensitivity in principle in the case where the rare spin spectrum contains little spectral information, the direct method has some practical advantages and has so far furnished almost all the high resolution double resonance NMR spectra in solids of rare spins.

For spins with I = 1/2, the MAS, CRAMPS etc. can result in high resolution NMR spectra. But most NMR active nuclei are quadrupole nuclei with I greater than 1/2. Those methods above are unable fully remove the broadening due to strong quadrupolar interactions. High resolution of solid state NMR for weak quadrupolar nuclei has not been obtained until recent years. Three years ago, A. Llor et. al. and A. Pines proposed and experimentally achieved independently the idea of dynamic angle spinning in which the spinner axis is made time dependent so that the second order broadening in sample spinning is attenuated, and achievement of high resolution NMR is obtained for half-integer spin quadrupolar nuclei with relatively small quadrupole moments.[22, 23] A. Pines also proposed and experimentally achieved the idea of double rotation in which the

sample spins about two axes simultaneously so that the second order broadening is eliminated.[24] Most quadrupole nuclei have a small gyromagnetic ratio and low natural abundance. In order to obtain large enough signal-to-noise ratio, a minimum amount of sample is required. The second method has the disadvantage of low filling factor. The dynamic angle spinning method seems more promising. In order to achieve high efficient dynamic angle spinning NMR spectra, the sample must spin fast enough (> 5 KHz) and be stable during the angle flipping, and the angle flipping time must be much shorter than T_1. MAS and CRAMPS also require a stable spinning system. So the first part of this work is to develop a stable system which can serve all those purposes.

THEORY OF HIGH RESOLUTION NMR IN SOLIDS

As shown in Eq. 1, anisotropic interactions are retained and dominate the NMR spectra of solids, and make them generally featureless. In order to extract useful information, one has to do some manipulations on the spin systems to suppress "unwanted" interactions and leave "wanted" interaction more-or-less unaffected. Eq. 2 shows that Hamiltonains consist of spatial parts and spin variable parts, so there are two ways to manipulate the spin systems. One is to rotate the samples to manipulate spatial parts of H and the other is to use multiple pulse to manipulate spin variables of H. A more detailed discussion follows.

I. Theory of line narrowing by sample spinning

In solids, there are several coordinate systems encountered when one wants to express some physical properties. Those coordinate systems are, usually in NMR, the principal axis system, the crystal frame, the rotation frame and the laboratory frame. Any two of these systems, i.e. (x,y,z) and (x',y',z') can be related by a unitary transformation $R(\alpha,\beta,\gamma)$ with the Euler angles (α,β,γ), i.e. for a given vector in two systems:

$$\vec{r}' = R\,\vec{r} \tag{3}$$

For a second rank tensor $\overleftrightarrow{R}$:

$$\mathcal{H}' = R\,\mathcal{H}\,R^{-1} \tag{4}$$

where $R(\alpha,\beta,\gamma)$ is defined as:

$$R(\alpha,\beta,\gamma) = R(\gamma)*R(\beta)*R(\alpha) \tag{5}$$

and

$$R(\alpha) = \begin{vmatrix} \cos\alpha & \sin\alpha & 0 \\ -\sin\alpha & \cos\alpha & 0 \\ 0 & 0 & 1 \end{vmatrix}$$

$$R(\beta) = \begin{vmatrix} \cos\beta & 0 & -\sin\beta \\ 0 & 1 & 0 \\ \sin\beta & 0 & \cos\beta \end{vmatrix} \tag{6}$$

$$R(\gamma) = \begin{vmatrix} \cos\gamma & \sin\gamma & 0 \\ -\sin\gamma & \cos\gamma & 0 \\ 0 & 0 & 1 \end{vmatrix}$$

When $\mathcal{H}$ is expressed in terms of irreducible spherical tensor operators as in Eq. 2, it is more convenient to use Wigner rotation matrices:

$$D^{(j)}_{mn}(\alpha,\beta,\gamma) = e^{-im\alpha}\, d^{(j)}_{mn}(\beta)\, e^{-in\gamma} \tag{7}$$

The unitary transformation (rotation) of a spherical tensor is expressed as

$$A'_{kq} = R(\alpha,\beta,\gamma)\ A_{kq}\ R^{-1}(\alpha,\beta,\gamma) = \sum_{p=-k}^{k} A_{kp}\ D^{(k)}_{pq}(\alpha,\beta,\gamma) \qquad (8)$$

For more information about the relation between $R(\alpha,\beta,\gamma)$ and $D^{(j)}_{mn}(\alpha,\beta,\gamma)$, refer to reference 25.

When the sample rotates in the magnetic field with the angular speed ω_r and the angle rotated $\phi(t) = \omega_r t+\phi_0$ (where ϕ_0 is initial angle), the Hamiltonian becomes time dependent:

$$H = \sum_{k=0}^{2} \sum_{q=-k}^{k} (-1)^q\ A_{kq}(t)\ T_{k,-q} \qquad (9)$$

where

$$A_{kq}(t) = \sum_{i,j=-k}^{k} A''_{kj}\ D^{(k)}_{ji}\ (\alpha,\beta,\gamma)\ D^{(k)}_{iq}\ (\phi(t),\theta,\psi,) \qquad (10)$$

where $D^{(k)}_{ij}(\alpha,\beta,\gamma)$ is the rotation which brings the principal axis system of tensor A'' on the rotation frame (in which the sample is static) and $D^{(k)}_{iq}\ (\phi(t),\theta,\psi,)$ is the rotation which brings the tensor A' in the rotation frame to the laboratory frame because all signals are detected at laboratory frame. The time dependence of $A_{kq}(t)$ is imposed by the sample spinning. For sufficiently rapid sample spinning, only the time average of the Hamiltonian contributes to the NMR spectrum. In the high field case usually encountered in NMR, non-secular terms can be neglected because they contribute little to the spectrum. The hamiltonian is modulated by sample rotation according to Eq. 7. All terms with $q \neq 0$ in Eq. 9 are averaged out. Eq. 9 reduces to

$$H = A_{00}\ T_{00} + A_{10}(\alpha,\beta,t)\ T_{10} + A_{20}(\alpha,\beta,t)\ T_{20} \qquad (11)$$

The antisymmetric part A_{10} of spin interactions does not contribute to the spectrum in first order approximation and can safely be neglected. The isotropic part $A_{00} = -(\sqrt{1}/3)\mathrm{Tr}\{A_{ij}\}$ is invariant under motion. According to Eq. 8:

$$A_{20}(\alpha,\beta,t) = \sum_{q=-2}^{2} A_2'^{q}(\alpha,\beta)\ e^{-i\omega_r t q}\ e^{-iq\phi_0}\ d^{(2)}_{q,0}(\theta) \qquad (12)$$

where θ is the angle between the spinner axis and the magnetic field B_0. $A_{20}(\alpha,\beta,t)$ is dependent on the orientation of each crystallite in the sample and gives rise to the powder broadening. If the rotation speed is not high enough ($\omega_r < A_{20}$), the A_{20} is modulated by the sample spinning, and rotational echos in the time domain (sidebands in the frequency domain) appear at multiples of the frequency $n\omega_r$ and $2n\omega_r$ away from the centerband [Fig. 8b]. If the rotation speed is high enough ($\omega_r >> A_{20}$), only the average of $A_{20}(t)$ contributes to the spectrum, all terms except with $q \neq 0$ in Eq. 11 are averaged out. For internal interactions being dipolar coupling, or shielding,

$$\bar{A}_{20}(\alpha,\beta,t) = \frac{1}{2}\ (3\cos^2\theta - 1)\ A'_{20}(\alpha,\beta) \qquad (13)$$

and

$$\bar{H} = A_{00}\ T_{00} + \frac{1}{2}\ (3\cos^2\theta - 1)\ A'_{20}(\alpha,\beta)T_{20} \qquad (14)$$

The linewidth is broadened by the second terms and scaled by a factor of $1/2(3\cos^2\theta - 1)$. If θ meets the magic angle condition $\theta_m = 54°44'$, the second term vanishes, and a liquid-like sharp isotropic peak obtained.

II. Theory of multiple pulse decoupling

The second approach to suppress "unwanted" interactions and extract useful information is to manipulate the spin variable part of Hamiltonian. In quantum mechanics, the evolution of a system under the influence of Hamiltonian H obeys Liouville-von Neumann equation:

$$i\frac{d\rho}{dt} = [H_{int} + H_{rf}, \rho] \tag{15}$$

where ρ is the density operator of the system. H_1 may be any type of Hamiltonian in Eq. 1, H_{rf} is the radiofrequency radiation (multiple pulses). Let the transformation

$$\rho = U_{rf}\,\tilde{\rho}\,U_{rf}^{+} \tag{16}$$

be made, in which one insists that U_{rf} obey the differential equation

$$i\frac{dU_{rf}}{dt} = H_{rf}\,U_{rf} \tag{17}$$

then inserting Eq. 16 to Eq. 15 yields the equation of motion of $\tilde{\rho}$

$$i\frac{d\tilde{\rho}}{dt} = [\tilde{H}_1, \tilde{\rho}] \tag{18}$$

where $\tilde{H}_1$ is

$$\tilde{H}_1 = U_{rf}^{+} H_1 U_{rf} \tag{19}$$

If a second transformation

$$\tilde{\rho} = U_{int} \tilde{\rho} \tilde{U}_{int}^{+} \tag{20}$$

is made, with U_{int} determined by

$$i\frac{dU_{int}}{dt} = \tilde{H}_{int} U_{int} \tag{21}$$

the equation of motion of $\tilde{\tilde{\rho}}$ is obtained

$$i\frac{d\tilde{\tilde{\rho}}}{dt} = [0, \tilde{\tilde{\rho}}] = 0 \tag{22}$$

This means that in the interaction frame of $\tilde{H}_1$, the spin system does not evolve

$$\tilde{\tilde{\rho}}(t) = \tilde{\tilde{\rho}}(0) \tag{23}$$

ρ and $\tilde{\tilde{\rho}}$ are related by the transformations

$$\rho = U_{rf}\, U_{int}\, \tilde{\tilde{\rho}}\, U_{int}^{-1} U_{rf}^{-1} \tag{24}$$

The evolution of ρ is governed by U_{rf} and U_1 which is implicitly governed by U_{rf} with Eq. 19 and Eq. 21.

If H_{rf} is chosen so that at a particular time t_c

$$U_{rf}(t_c) = U_1(t_c) = 1 \tag{25}$$

Then

$$\rho(t_c) = \tilde{\tilde{\rho}}(t_c) = \tilde{\tilde{\rho}}(0) = \rho(0) \tag{26}$$

This indicates that the H_1 does not affect the evolution of the spin system, in another words, the influence of H_1 is "removed" by manipulation of H_{rf}.

U can be calculated by Dyson expression

$$U = T \exp\{-i\int_0^t H(t')dt'\} \tag{27}$$

where T is time ordering operator, or by the Magnus Expression

$$U = \exp\{-i[\bar{H}^{(0)} + \bar{H}^{(1)} + \bar{H}^{(2)} + \ldots]\} \tag{28}$$

where

$$\bar{H}^{(0)} = \frac{1}{t_c} \int_0^t H(t')dt' \tag{29}$$

$$\bar{H}^{(1)} = \frac{-i}{2t_c} \int_0^t dt' [H(t'), \int_0^{t'} dt'' H(t'')] \tag{30}$$

$\bar{H}^{(2)} = \ldots$

For the details of calculation of U, refer to reference [26].

The WAHUHA-4 pulse sequence, MREV-8 pulse sequence and BR-24 pulse sequence can be used to remove homonuclear dipolar interactions. A number of other pulse sequences have been designed for variable purposes which make solid state NMR more flexible and useful in research.

In some cases (like ^{1}H and ^{19}F), the problem of overlapping of tensors still remains after removing dipolar interactions by multiple pulse decoupling and the different components in the sample cannot be identified uniquely. This can be overcome by combining magic angle spinning and multiple pulse decoupling,[18] which is termed CRAMPS (Combined Rotation And Multiple-Pulse Spectroscopy). Then resolution of 2 ppm is achievable (Fig. 9).

III. Theory of dynamic angle spinning and double rotor spinning

MAS is sufficient to average out the anisotropy of chemical shifts and weak dipolar interactions at normal spinning speeds (5~10 KHz) to first order in perturbation theory. Multiple pulse decoupling is sufficient to remove dipolar interactions. For a quadrupolar nuclear spin system at high magnetic fields, the second order contribution is dominant in the line broadening. MAS provides only a fourfold reduction in line width.[27]

For a quadrupolar nuclei in many solids, the dipolar broadening is much smaller than the second order quadrupole broadening of the central transition. In such a case, the powder pattern associated

with the outer transitions (+1/2 ⇔ +3/2, etc) is broadened to first order, and is unobservable, the central transition (1/2 ⇔ -1/2) can be considered as that of a "fictitious spin 1/2". A second order quadrupolar shift will then be superimposed on any isotropic chemical shift.

$$H = I_z[\omega_0 + A\ (\theta,\phi)] \tag{31}$$

with

$$A(\theta,\phi) = 2\pi\nu_Q^{(2)} \tag{32}$$

$\nu_Q^{(2)}$ can be expressed in terms of Wigner rotation matrices $D^{(l)}_{m',m}$, which only with $l = 0,2,4$ and m,m' even are used.[7] Under sample rotation,

$$\nu_Q^{(2)}(1/2 \Leftrightarrow -1/2) = \frac{\nu_Q^2}{\nu_0}\left[I(I+1) - \frac{3}{4}\right] \sum_{k=0}^{2} \sum_{m,n=-k}^{k} \left[\sum_{p=-k}^{k} A''_{2k,2p} D^{(2k)}_{2p,2n}(\alpha,\beta,\gamma) \right] D^{(2k)}_{2n,2m}(\phi(t),\theta,0) \tag{33}$$

where $D^{(2k)}_{2p,2n}(\alpha,\beta,\gamma)$ is the rotation which aligns the principal axis system of the quadrupolar tensor with the rotation frame and $D^{(2k)}_{2n,2m}(\phi(t),\theta,0)$ describes rotation in the laboratory frame at an angle θ to the B_0 field (Z axis) with rotation frequency ω_r such that $\phi(t) = \omega_r t$. When the sample rotates fast enough, all terms in Eq. 33 with $n,m \neq 0$ are averaged out and Eq. 33 reduces to

$$\nu_Q^{(2)}(1/2 \Leftrightarrow -1/2) = \frac{\nu_Q^2}{\nu_0}\left[I(I+1) - \frac{3}{4}\right]\sum_{k=0}^{2}\left[\sum_{p=-k}^{k} A_{2k,2p} D^{2k)}_{2p,0}(\alpha,\beta)\right] D^{(2k)}_{0,0}(\theta)$$

$$= \frac{\nu_Q^2}{\nu_0}\left[I(I+1) - \frac{3}{4}\right]*\left[A_{00} + B_{20}(\alpha,\beta) d^2_{00}(\theta) + B_{40} d^4_{00}(\theta)\right] \quad (34)$$

where

$$d^2_{00}(\theta) = 1/2(3\cos^2\theta - 1) \quad (35)$$

and

$$d^4_{00}(\theta) = 1/2(35\cos^4\theta - 30\cos^2\theta + 3) \quad (36)$$

A_{00} is a constant, whereas $B_{20}(\alpha,\beta)$ and $B_{40}(\alpha,\beta)$ are dependent on the orientation of each crystallite in the sample and give rise to the powder broadening. Clearly, there is no rotation about a unique angle which can average out at the same time both the d^2_{00} and d^4_{00} terms. Multiple angle spinning is the only way to cancel these two terms. There are two ways to achieve this. One is the way of dynamic angle spinning in which the sample spins at two different angles θ_1 and θ_2.[22, 23] θ_1 and θ_2 are chosen to fulfill the following conditions at same time:

$$d^2_{00}(\theta_1) = - d^2_{00}(\theta_2)$$

$$d^4_{00}(\theta_1) = - d^4_{00}(\theta_2) \tag{37}$$

that is $\theta_1 = 37.38°$ and $\theta_2 = 79.19°$. One can rotate the sample for some time about angle θ_1, the spin system will evolve under the influence of $\nu_Q^{(2)}(\theta_1)$; and then rotate the sample the same time about the angle θ_2. The spin system will evolve under the influence of $\nu_Q^{(2)}(\theta_2)$. The anisotropic shift of each spin is sign reversed when shifting from θ_1 to θ_2 because of condition Eq. 37 so that the anisotropic dephasing (different for each crystallite) which is accumulated during the first evolution period is cancelled during the second evolution period whereas the isotropic dephasing accumulates, an echo occurs at the end of this evolution period whose amplitude is modulated by the isotropic shift only.

One can also use double rotor spinning to cancel d^2_{00} and d^4_{00}.[24] One rotor spins at the angle θ_1 which meets the condition of

$$d^2_{00}(\theta_1) = 1/2\ (3\cos^2\theta_1 - 1) = 0 \tag{38}$$

$\theta_1 = 54.73°$ which is the "magic angle". Another rotor rotates at the angle θ_2 which meets the condition of

$$d^4_{00}(\theta_2) = 1/8\ (35\cos^4\theta_2 - 30\cos^2\theta_2 + 3) = 0 \tag{39}$$

Eq. 39 has two solutions: $\theta_2 = 30.6°$ or $\theta_2 = 70.1°$. One rotor is embedded in the other, the axis of inner rotor is inclined by θ_i with respect to the axis of outer rotor. The spinning axis of outer rotor forms an angle θ_o with respect to the direction of the magnetic field, where either

$$\theta_i = \theta_1, \ \theta_o = \theta_2$$

or

$$\theta_i = \theta_2, \ \theta_o = \theta_1$$

The anisotropic part of $\nu_Q^{(2)}$ can be averaged to zero by those two methods, and high resolution NMR for quadrupole nuclei can be achieved. The double rotor spinning method has the disadvantage of low filling factor which will reduce the sensitivity and signal/noise ratio, this is critical in quadrupolar nuclear NMR because of low natural abundance and small gyromagnetic ratio. The dynamic angle spinning seems more promising, hence more interesting to us.

THE DESIGN OF DOUBLE BEARING PROBE

The design of rotor-stator system determines the efficiency of sample spinning and the stability during the angle flipping. A popular design of stator for sample spinning is the Windmill single bearing stator.[28] In general, there are three kinds of motion of cylindrical spinners inside of the stator during spinning pointed out by Doty and Eillis shown in Fig. 1:[29]

1. the spinner spins about its axis.
2. the axis of the spinner spins about the axis of the stator which is called the cylindrical mode.
3. the axis of the spinner precesses about the axis of the stator which is called the conical mode.

The second and the third modes affect the spinning speed and make the spinning unstable. In single bearing stator, one end of the spinner is loose, so the conical mode is the major factor affecting spinning. In order to enhance the speed and stability of spinning, one must effectively suppress the conical and cylindrical modes. The best way to accomplish this is to add another bearing at other end of the spinner. Based on this ideal, the design of our new type of double bearing stator is shown in Fig. 2-5. The stator consists of four parts: (1) a low driving and bearing part, (2) a top bearing part, (3) a bottom bearing part, (4) outside housing. The design of the driving end of the rotor-stator system is similar to that published by Wind et al.,[28] but now the unit is equipped with a double bearing and is enclosed in a brass cylinder, machined

with an access, as shown in Fig. 2-3, for exit of bearing gas, and for insertion of a free standing NMR coil. The structure of the spinner is shown in Fig. 4. Stability of spinning is achieved not only by separate bearings at both ends of the cylindrical rotor, but also by supplying an air bearing to the bottom of rotor, an adaptation similar to the one recently reported for use in spinning large (2 cm^3) sample volumes.[30] Separate air drives are supplied for side bearings, drive, and bottom bearing. The bottom bearing gas passes through a 1-72 brass screw, with a gap between the spinner and bearing surface of the screw being adjustable for optimal operation (Fig. 5). The spinner is made of Torlon™ when high magic angle spinning (MAS) speeds are required and for observation of ^{19}F, or Kel-F™ for measurements on ^{1}H. Similarly, support for the bottom bearing and drive, and top bearing assembly is either polycarbonate or Kel-F™. Standard machining procedures are used to provide optimal alignment between the axis of rotation and the cylindrical side bearing surfaces. Fig. 6 is the assembly of the probe. A spinning frequency of 10KHz is easily attainable with a 5-mm-o.d. spinner made of Torlon™ using air pressures of 10^5Pa (15psi), $7x10^4$Pa (10psi), and $3.3X10^5$Pa (50psi), for side and bottom bearings, and drive, respectively. Speeds to 16KHz have been achieved in our laboratory with this arrangement. The rf portion is either a tapped series tuned circuit[31] or some other configuration depending upon the frequency range of interest, and the number of different resonance frequencies desired in a single coil circuit.[32]

THE PERFORMANCE OF THE PROBE

The performance of the probe is shown by the NMR spectra in Fig. 7 to Fig. 9. Fig. 7 is the static spectrum of Ag_2F which has axial symmetric Knight shift tensor. Fig. 8 is the static and MAS spectra of BaF_2 and Fig. 9 is the CRAMPS spectrum (MAS and homonuclear decoupling) of the fluorine in yttrium oxyfluoride (YOF). CRAMPS spectrum was obtained at a spinning speed of ~4.25 KHz (for homonuclear decoupling, higher speeds begin to interfere with the averaging condition in spin space[2]). The static full width at half height (FWHH) of ^{19}F in YOF is 32.5 KHZ. These spectra were obtained using a Bruker MSL-300 console and magnent with the resonance frequency of 288.23MHz. C_6F_6 is used as a reference.

Stability of spinning to a rapid (~9 ms) change in orientation of the axis of rotation by 45° is demonstrated in Fig. 10 which is a photo of a light-detected signal from the spinner, plotted as a function of time, monitored in a transient recorder and played back to an oscilloscope from the memory of the recorder. Fig. 10a is an expanded version of Fig. 10b, showing both short- and long-term stability when the sample orientation is changed. The oscillations and dc offset of the signal result from movement of the spinner within the path of the light detector, and serve to mark event timing. The spinner is seen to "ring" for about 25 ms after reorientation, but the spinning speed itself remains constant to

better than our measurement accuracy of 1% over the time period of the reorientation event.

CONCLUSION

The probe meets the requirements for sufficient B_1 homogeneity for homonuclear decoupling of strongly dipolar coupled solids, ease, and stability of spinning to speeds of 10 KHz in compact configuration, and stability to rapid (9 ms) changes in axis of rotation by as much as 45°, being therefore suitable for dynamic angle spinning (DAS) experiments designed to attenuate second order quadrupolar broadening in NMR of half spin quadrupolar nuclei. where values of T_1 are not less than 50 ms.

ACKNOWLEDGEMENT

Steve Dec of Colorado State University was especially helpful with hints in the art of constructing the Wind-type spinning arrangement.(10)

REFERENCES

1. T. C. Farrar and E. D. Becker, Pulse and fourier Transform NMR (Academic,New York, 1971).
2. B. C. Gerstein and C. R. Dybowski, Transient Techniques in NMR of Solids (Academic, New York, 1985).
3. U. Haeberlen, High Resolution NMR in Solids, Selective Averaging (Academic New York,1976).
4. M. Mehring, High Resolution NMR Spectroscopy in Solids (Springer, Heideberg, 1976)
5. R. H. Ernst, G. Bodenhausen, and A. Waukon, Principles of Magnetic Resonance in One and Two Dimensions (Oxford, UK,1987).
6. M. Munowitz, Coherence and NMR (Wiley, New York,1988).
7. A. Llor and J. Virlet, Chem. Phys. Lett. **152**, 248 (1988).
8. I. J. Lowe, Phys. Rev. Lett. **2**, 285 (1959).
9. E. R. Andrew, Prog. NMR Spectrosc. **8**, 1 (1971).
10. S. F. Dec, R. A. Wind, G. E. Maciel, and F. E. Anthonio, J. Magn. Reson. **70**, 355 (1986).
11. Chemagnetics, Inc., 208 Commerce Drive, Ft. Collins, CO 80524.
12. Doty Scientific, 600 Clemson Road, Columbia, South Carolina 29223.
13. A. Abragam:The Principles of Nuclear Magnetism. London, Oxford Univ. Press 1961
14. a). E. R. Andrew, R. G. Eades, Prooc. Roy. Soc. London **A216**, 398 (1953).

b). E. R. Andrew, S. Clough, L. F. Farnell, T. D. Gledhill, I. Roberts, Phys. Letters **19**, 6 (1966).

15. J. S. Waugh, L. M. Huber, U. Haeberlein, Phys. Rev. Letters **20**, 180(1968).

16. P. Mansfield. Phys. Lett. **A32**, 485 (1970).

17. W. K. Rhim, D. D. Elleman & R. W. Vaughan, J. Chem. Phys. **59**, 3740 (1973).

18. a). B. C. Gerstein, C. Chow, R. G. Pembleton & R. C. Wilson J. Phys. Chem. **81**, 565 (1977)

b). B. C. Gerstein, R. G. Pembleton, R. C. Wilson & L. M. Ryan, J. Chem. Phys. **66**, 361 (1977).

19. a). S. R. Hartmann, E. L. Hahn, Phys. Rev. **128**, 2042 (1962).

b). E. P. Jones, S. R. Hartmann, Phys. Rev. **36**, 757 (1972).

20. a). F. M. Lurie, C. P. Slichter, Phys. Rev. **133**, A1108 (1964).

b). C. P. Slichter, W. C. Holton, Phys.Rev. **122** 1701 (1961).

21. a). A. Pines, M. G. Gibby, J. S. Waugh, J. Chem. Phys. **56**, 1776 (1972).

b). A. Pines, M. G. Gibby, J. S. Waugh, J. Chem. Phys. **59**, 569 (1973).

c). A. Pines, M. G. Gibby, J. S. Waugh, J. Chem. Phys. letters **15**, 373(1972).

22. A. Llor and J. Virlet, in: Ninth Experimental NMR Conference, Bad Aussee, Austria (May 1988).

23. A. Pines, in: Ninth Experimental NMR Conference, Bad Aussee, Austria (May 1988).

24. A. Samoson and A. Pines, Rev. Sci. Instrum. **60**(10), 3239 (1990).

25. M. E. Rose, "Elementary Theory of Angular Momentum", New York, John Wiley & Sons, Inc. London 1963.

26. B. C. Gerstein and C. R. Dybowski, "Transient Techniques in NMR of Solids", Academic Press, Inc. Orland, Florida 32887, 1985.

27. A. Samoson, E. Kundla, Abstracts of the Fifth Specialized Colloque AMPERE, Uppsala, 1981, p.37.

28. R. A. Wind et al., J. Magn. Reson. **52**, 424 (1983).

29. D. Doty and P. Eillis, Rev. Sci. Instrum. **52**(12), 1868 (1981).

30. M. Zhang and G. E. Maciel, J. Magn. Reson., **85**, 156 (1989).

31. P. D. Murphy and B. C. Gerstein, Analysis and computerized Design of NMR Probe Circuit, Ames Laboratory Report IS-4436, UC-13 (1978).

32. R. A. Mckay, "Quadrupole Tuned Magic Angle Spinning NMR Probe", Abstract, 31st ENC, Asilomar, CA, April 1-5, 1990.

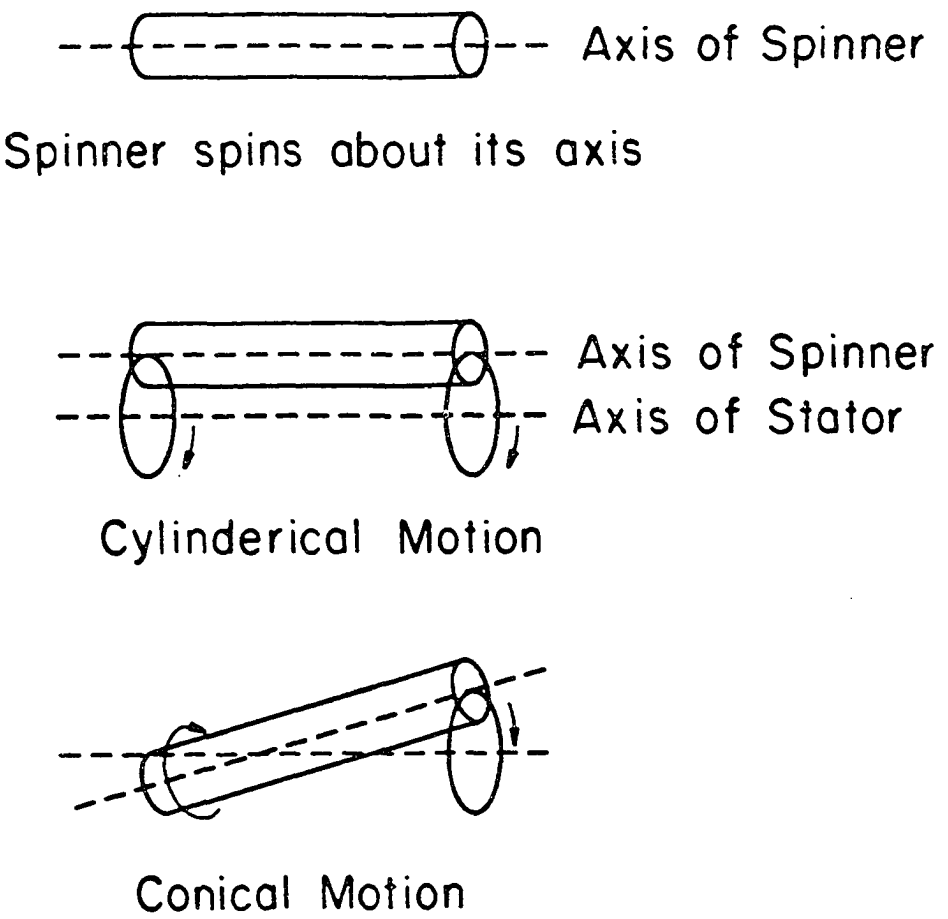

Figure 1: Three modes of motion of a cylindrical spinner.

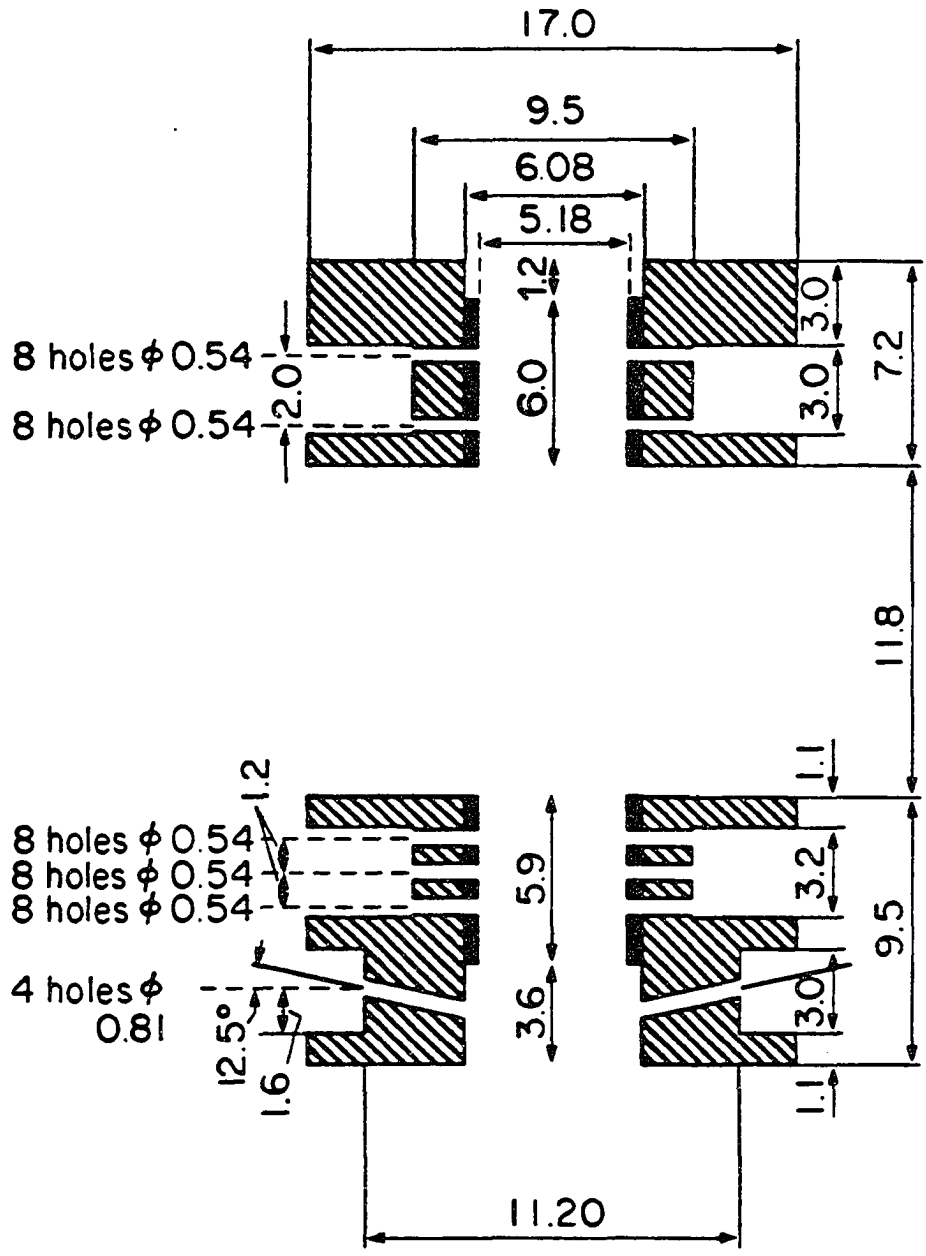

Figure 2: Details of the drive and side bearing assemblies. Inner surface (black), brass; outer portions, Kel-F™ or polycarbonate.

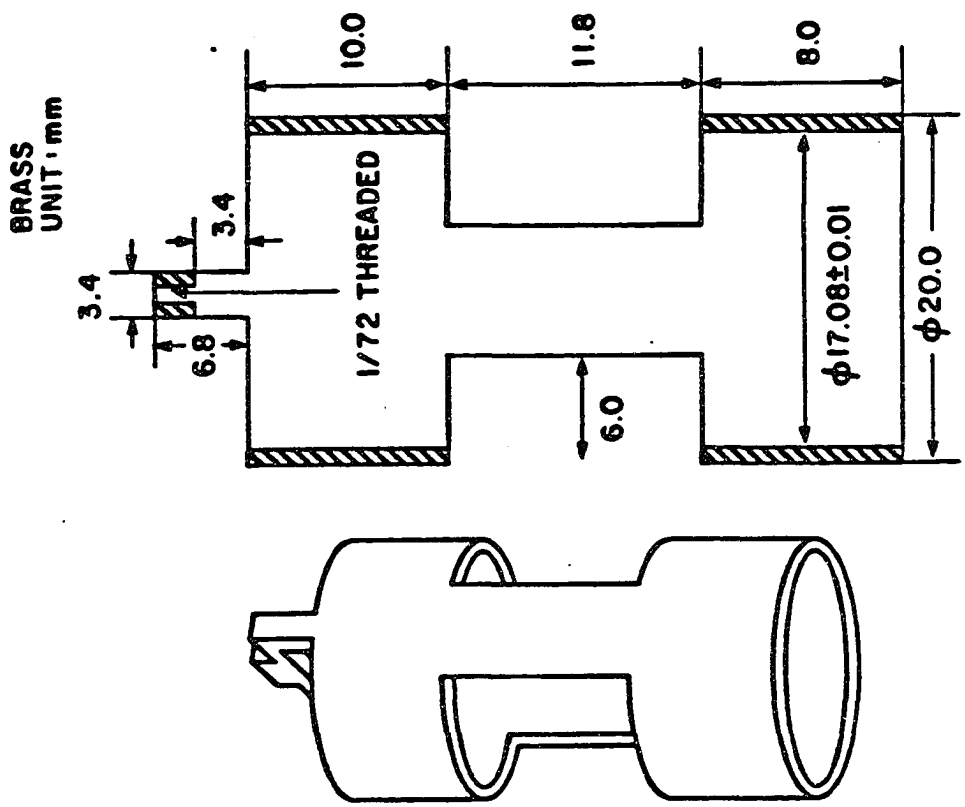

Figure 3: The outside housing (brass).

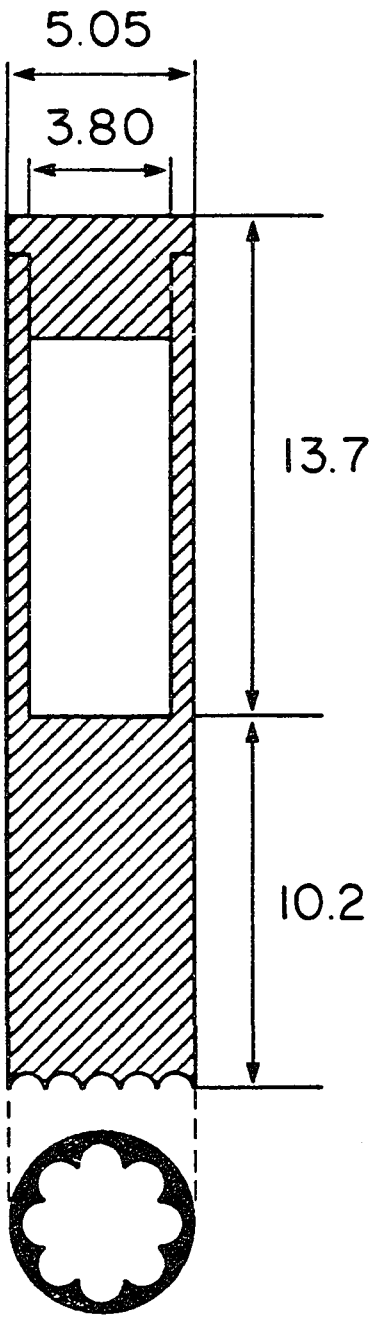

Figure 4: The structure of spinner (Torlon^{TM} or Kel-F^{TM}).

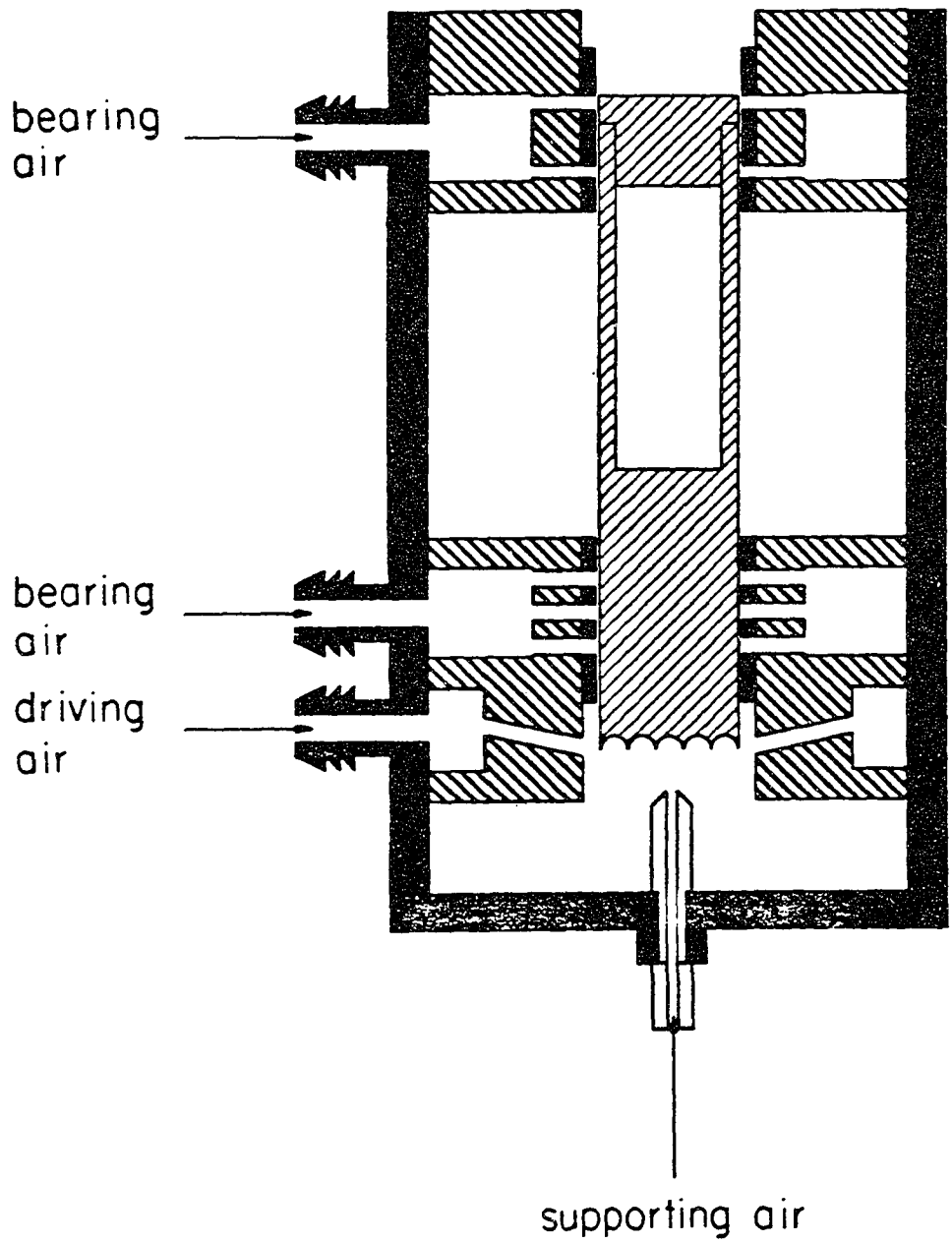

Figure 5: Cross section of the entire stator and spinner assembly.

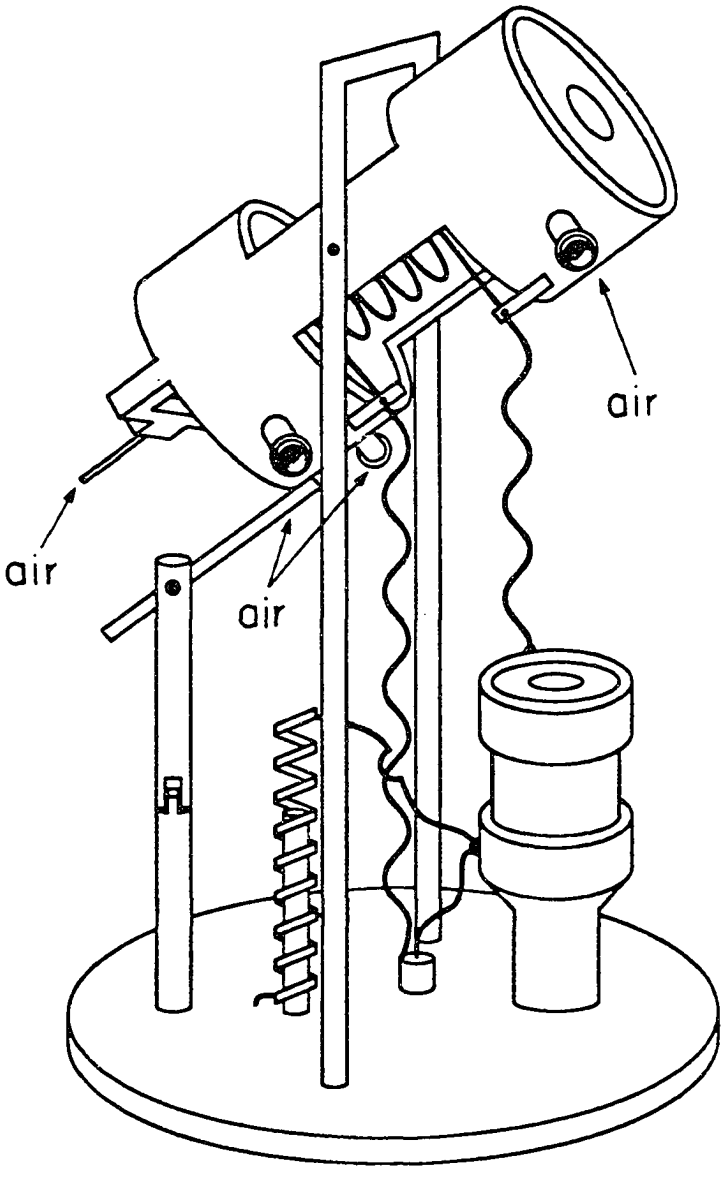

Figure 6: Probe assembly.

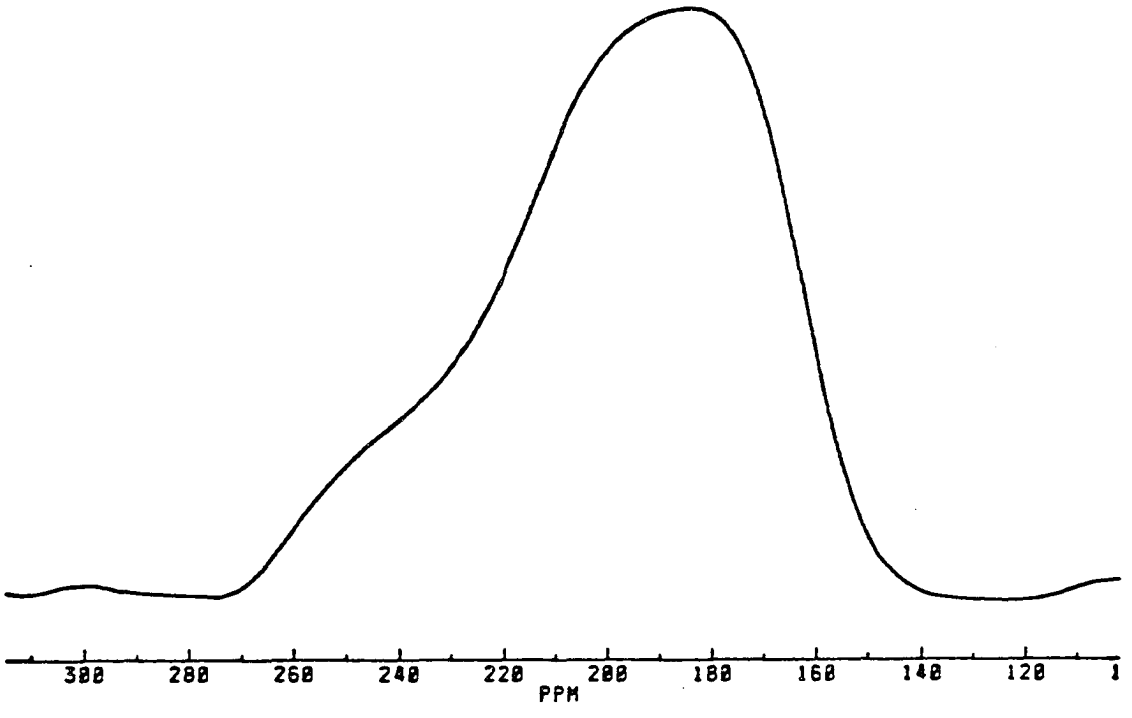

Figure 7: Static NMR spectrum of ^{19}F in Ag_2F

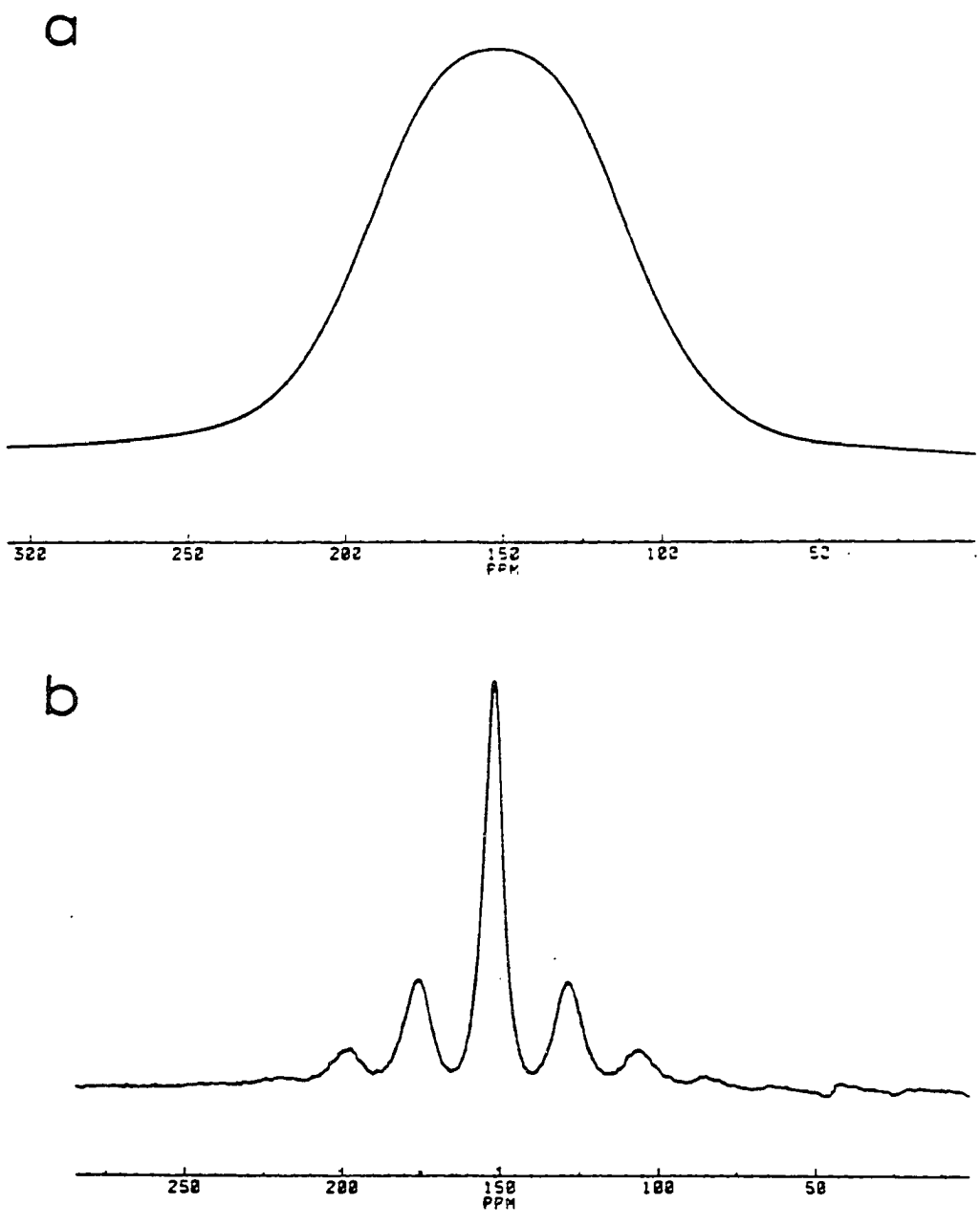

Figure 8: NMR spectra of ^{19}F in BaF_2. (a) Static, (b) MAS.

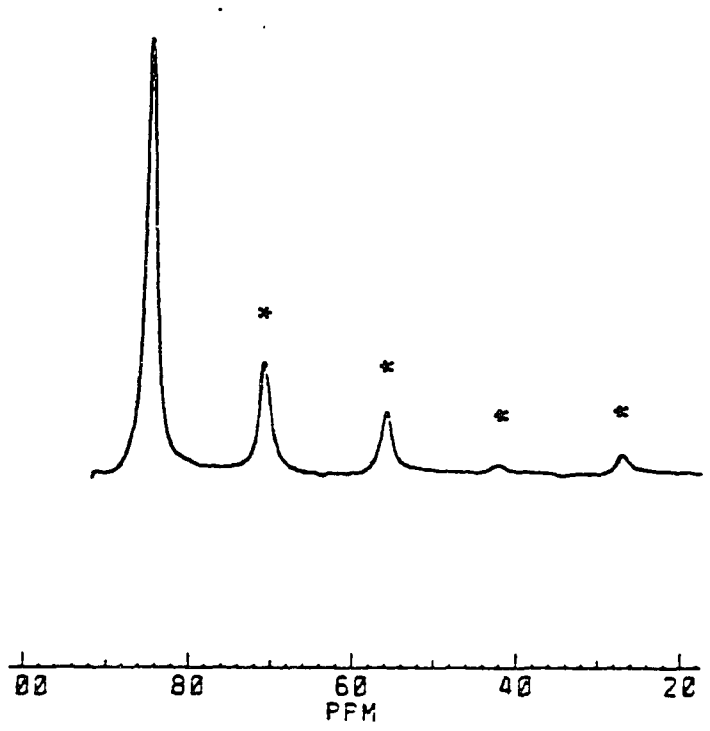

Figure 9: CRAMPS spectrum of ^{19}F in YOF. Asterisks (*) mark spinning sidebands.

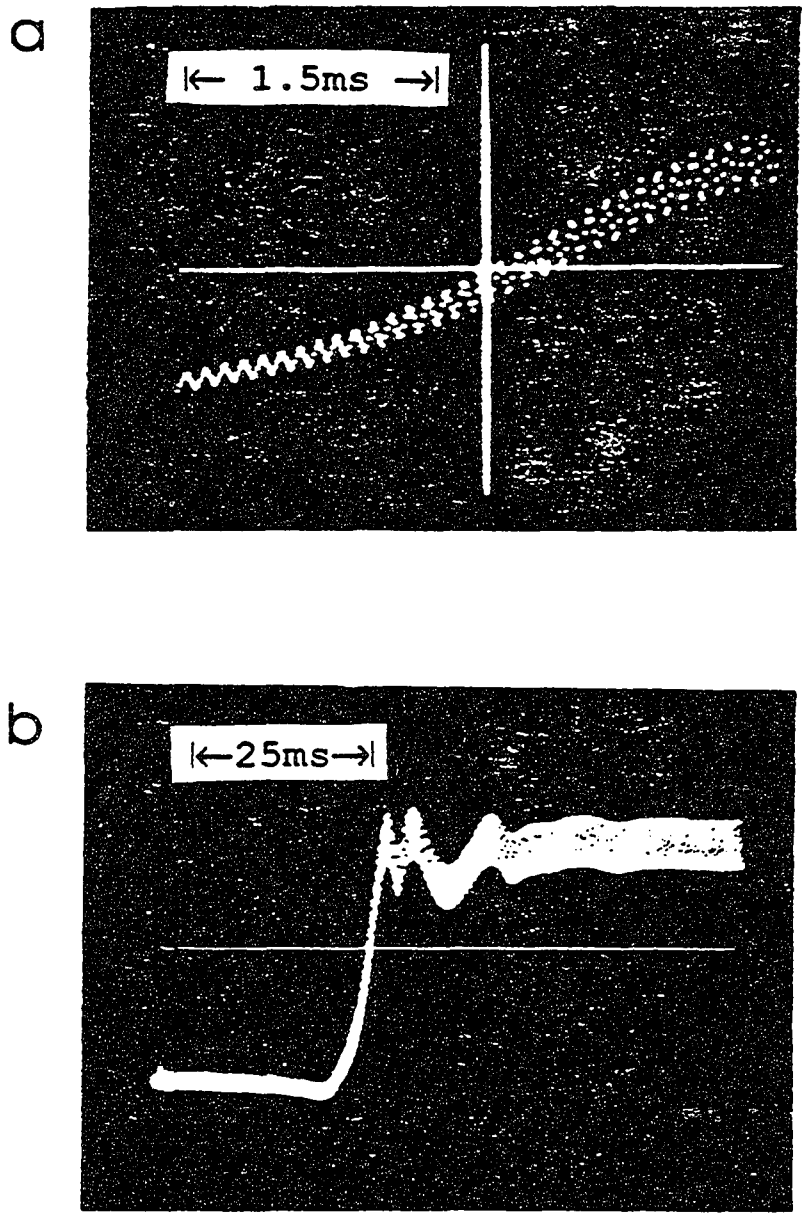

Figure 10: Stability of rotation under a rapid (~9 ms) change in orientation by 45°. (a) 3.7 ms of period during center of rotational reorientation. The light-detected oscillations seen during the scan have the frequency of the spinner. (b) 60-ms scan showing rotation speed before, during and after change in orientation. The assembly "rings" for about 25 ms after reorientation.

ACKNOWLEDGEMENTS

All achievements are devoted to my wife, who is my greatest asset, Wenrong. She supported me to finish this work with all her love and care, and took care of all housework without complaint.

I wish to sincerely thank Dr. Bernard C. Gerstein for his scientific guidance, enthusiastic encouragement and friendship throughout the years. His spirit of devoting his love, kindness and care to the younger generation is specially appreciated.

I wish to thank Dr. Marek Pruski, Dr. Hans R. Loeliger, Dr. Vinco Rutar and Dr. David Torgeson for their friendship, great help, cooperation and discussion throughout this work.

I also like to thank Dr. Po-Jin Chu, Dr. William Shao, Miss Luisita C. Dela Rosa, Mr. Sonjong Hwuang and Mr. Hosseini Sadri for their friendship and beneficial discussions.

Finally I like to thank all my friends in Ames who made my life happy and enjoyable.

This work was performed at Ames Laboratory under contract No. W-7405-eng-82 with the U. S. Department of Energy. The United States government has assigned the DOE Report number IS-T 1546 to this thesis.